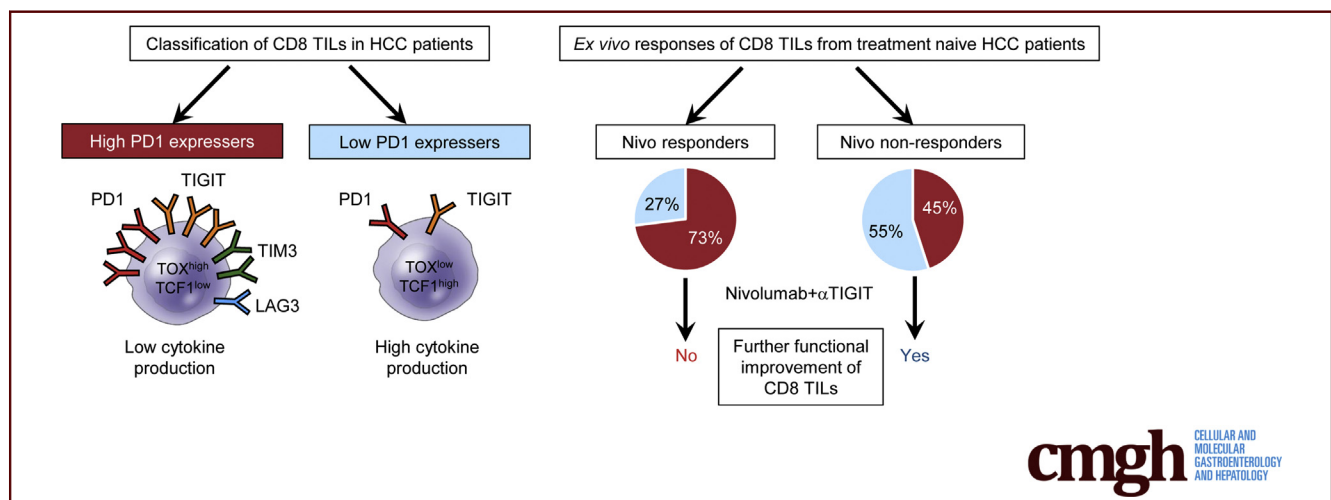# cmgh

ORIGINAL RESEARCH

TIGIT and PD1 Co-blockade Restores ex vivo Functions of Human Tumor-Infiltrating CD8+ T Cells in Hepatocellular Carcinoma

Zhouhong Ge,[1] Guoying Zhou,[1] Lucia Campos Carrascosa,[1] Erik Gausvik,[1] Patrick P. C. Boor,[1] Lisanne Noordam,[1] Michael Doukas,[2] Wojciech G. Polak,[3] Türkan Terkivatan,[3] Qiuwei Pan,[1] R. Bart Takkenberg,[4] Joanne Verheij,[5] Joris I. Erdmann,[6] Jan N. M. IJzermans,[3] Maikel P. Peppelenbosch,[1] Jaco Kraan,[7] Jaap Kwekkeboom,[1,b] and Dave Sprengers[1,b]

[1]Department of Gastroenterology and Hepatology, Erasmus MC-University Medical Center, [2]Department of Pathology, Erasmus MC-University Medical Center, [3]Department of Surgery, Erasmus MC-University Medical Center, and [7]Department of Medical Oncology, Erasmus MC-University Medical Center, Rotterdam, the Netherlands; and [4]Department of Gastroenterology and Hepatology, Amsterdam UMC location AMC, [5]Department of Pathology, Amsterdam UMC location AMC, and [6]Department of Surgery, Amsterdam UMC location AMC, Amsterdam, the Netherlands

SUMMARY

CD8+ TILs that contain terminally exhausted PD1high CD8+ cells generally respond to ex vivo single PD1 blockade, whereas CD8+ TILs of most HCC patients without this subset do not respond to single PD1 blockade but can be functionally restored by ex vivo co-blockade of TIGIT and PD1.

BACKGROUND & AIMS: TIGIT is a co-inhibitory receptor, and its suitability as a target for cancer immunotherapy in HCC is unknown. PD1 blockade is clinically effective in about 20% of advanced HCC patients. Here we aim to determine whether co-blockade of TIGIT/PD1 has added value to restore functionality of HCC tumor-infiltrating T cells (TILs).

METHODS: Mononuclear leukocytes were isolated from tumors, paired tumor-free liver tissues (TFL) and peripheral blood of HCC patients, and used for flow cytometric phenotyping and functional assays. CD3/CD28 T-cell stimulation and antigen-specific assays were used to study the ex vivo effects of TIGIT/PD1 single or dual blockade on T-cell functions.

RESULTS: TIGIT was enriched, whereas its co-stimulatory counterpart CD226 was down-regulated on PD1high CD8+ TILs. PD1high TIGIT+ CD8+ TILs co-expressed exhaustion markers TIM3 and LAG3 and demonstrated higher TOX expression. Furthermore, this subset showed decreased capacity to produce IFN-γ and TNF-α. Expression of TIGIT-ligand CD155 was up-regulated on tumor cells compared with hepatocytes in TFL. Whereas single PD1 blockade preferentially enhanced ex vivo functions of CD8+ TILs from tumors with PD1high CD8+ TILs (high PD1 expressers), co-blockade of TIGIT and PD1 improved proliferation and cytokine production of CD8+ TILs from tumors enriched for PD1int CD8+ TILs (low PD1 expressers). Importantly, ex vivo co-blockade of TIGIT/PD1 improved proliferation, cytokine production, and cytotoxicity of CD8+ TILs compared with single PD1 blockade.

CONCLUSIONS: Ex vivo, co-blockade of TIGIT/PD1 improves functionality of CD8+ TILs that do not respond to single PD1 blockade. Therefore co-blockade of TIGIT/PD1 could be a promising immune therapeutic strategy for HCC patients. (Cell Mol Gastroenterol Hepatol 2021;12:443–464; https://doi.org/10.1016/j.jcmgh.2021.03.003)

Keywords: TIGIT; CD226; TOX; HCC; Immunotherapy.

Liver cancer is the sixth most common cancer and the fourth most frequent cause of cancer-related death worldwide in 2018.[1] Hepatocellular carcinoma (HCC) comprises 75%–85% of all liver cancer cases.[1] Most patients are diagnosed at a late stage, and their median survival is less than 2 years.[2] Efforts are underway to identify new therapies for the treatment of advanced HCC. Recently, cancer immunotherapies targeting the co-inhibitory programmed cell death protein 1 (PD1)/programmed death-ligand 1 (PD-L1) pathway achieved survival benefit in multiple cancers, with the Food and Drug Administration approval of anti-PD1 antibody nivolumab for HCC treatment in 2017[3] and pembrolizumab in 2018.[4]

Anti-PD1 therapy results in objective response rates of 16%–20% in patients with advanced HCC[3,4] but does not prolong survival in HCC patients previously treated with sorafenib.[5] In an effort to improve the response rate of anti-PD1 therapy, combination therapies with blockade of other inhibitory immune checkpoints are being investigated. Anti-PD1/PD-L1 treatment in combination with anti-cytotoxic T-lymphocyte associated protein 4 is highly efficacious in melanoma and advanced non–small-cell lung cancer.[6–8] The combination of anti-PD1 with anti-cell immunoglobulin and mucin domain 3 (TIM-3)[9,10] has demonstrated promising results in preclinical studies. Our group previously found that the combined blockade of PD-L1 with TIM3, lymphocyte-activation gene 3 (LAG3), or cytotoxic T-lymphocyte associated protein 4 further restored responses of human HCC tumor-derived T cells to tumor-associated antigens (TAAs) in ex vivo assays compared with single PD-L1 blockade.[11]

T-cell immune receptor with immunoglobulin and ITIM domains (TIGIT) is a novel co-inhibitory molecule in cancer immunotherapy. TIGIT has a co-stimulatory counterpart called CD226 (DNAM-1). Both are expressed on multiple immune cell subsets, including activated and memory T cells, regulatory T cells (Treg), and natural killer cells.[12–15] These 2 receptors share the same ligand CD155 (also known as PVR, poliovirus receptor), but TIGIT has higher affinity for CD155. CD155 is highly expressed on dendritic cells, fibroblasts, endothelial cells, and some tumor cells.[12,16,17] It has been shown that TIGIT exerts immunosuppressive functions by inhibiting interleukin 12 and enhancing interleukin 10 production by dendritic cells through CD155, thereby inhibiting CD4$^+$ T-cell proliferation and interferon (IFN)-γ production.[12] Furthermore, TIGIT can directly suppress T-cell functions by cell-intrinsic inhibitory signaling.[18] Finally, TIGIT can compete for ligand binding with CD226, thereby reducing T-cell co-stimulation via CD226,[19] and can prevent co-stimulatory signaling via CD226 by blocking CD226 homodimerization.[20]

Interestingly, TIGIT is expressed on tumor-infiltrating T cells (TILs) in several types of human tumors, and its expression on TILs correlates with PD1 expression.[20–22] TIGIT and PD1 were also found to be co-expressed on tumor antigen–specific CD8$^+$ T cells from melanoma patients,[23] and dual TIGIT/PD-L1 blockade synergistically elicits tumor rejection in mouse cancer models[20,24] and increases in vitro proliferation and cytokine production of tumor antigen–specific CD8$^+$ T cells from melanoma patients.[23] Therefore, clinical trials on co-blockade of TIGIT with PD1/PD-L1 in multiple solid tumors are ongoing (BMS: NCT02913313, Genetech: NCT02794571, NCT03563716, Oncomed: NCT03119428).

To which extent TIGIT is expressed on TILs of HCC patients and whether TIGIT blockade alone or in combination with PD1 blockade can reinvigorate TILs of HCC patients is still unknown. Here, we compared expression of TIGIT and its co-stimulatory counterpart CD226 on T cells isolated from tumors, paired tumor-free liver tissues (TFLs), and peripheral blood of HCC patients, characterized TIGIT-expressing CD8$^+$ TILs, and studied the effects of single and combined TIGIT/PD1 blockade on ex vivo TIL responses.

Results

TIGIT/CD226 Ratio Is Increased on Intratumoral CD8$^+$ T and Treg Cells

We compared the expression of TIGIT and CD226 on CD8$^+$ T cells, CD4$^+$FOXP3$^+$ Treg, and CD4$^+$FOXP3$^-$ Th cells in HCC tumors, paired TFLs, and blood. Gating strategy is shown in Figure 1A. In all tissue compartments, TIGIT was expressed on CD8$^+$ T cells and Th, whereas the highest expression was found on Treg (Figure 2A–D). In contrast, compared with TFLs and blood, significantly reduced proportions of CD8$^+$ T and Treg in tumor expressed CD226 (Figure 1B, Figure 2A–D). In addition, the median fluorescent intensities (MFIs) of TIGIT on CD8$^+$, Treg, and Th cells in tumor and TFLs did not differ much, whereas the MFI of CD226 was considerably decreased in tumor compared with TFLs (Figure 1C and D). As a result, ratios of TIGIT/CD226 frequencies and MFIs of both CD8$^+$ T and Treg were highest in the tumor (Figure 1E, Figure 2E). We observed limited co-expression of TIGIT and CD226 on T-cell subsets in all 3 tissue compartments (Figure 2F). Importantly, the TIGIT$^+$CD226$^-$ T-cell fractions were increased significantly in Treg and Th in the tumor compared with TFLs (Figure 1F).

These data suggest that tumor-infiltrating CD8$^+$ T cells receive mainly co-inhibitory signals (via TIGIT) and fewer co-stimulatory signals (via CD226) from CD155-expressing cells. In addition, increased TIGIT/CD226 ratios on Treg may enable Treg to be highly sensitive to TIGIT signals that can enhance their suppressive function.[25]

[b]Authors share co-senior authorship.
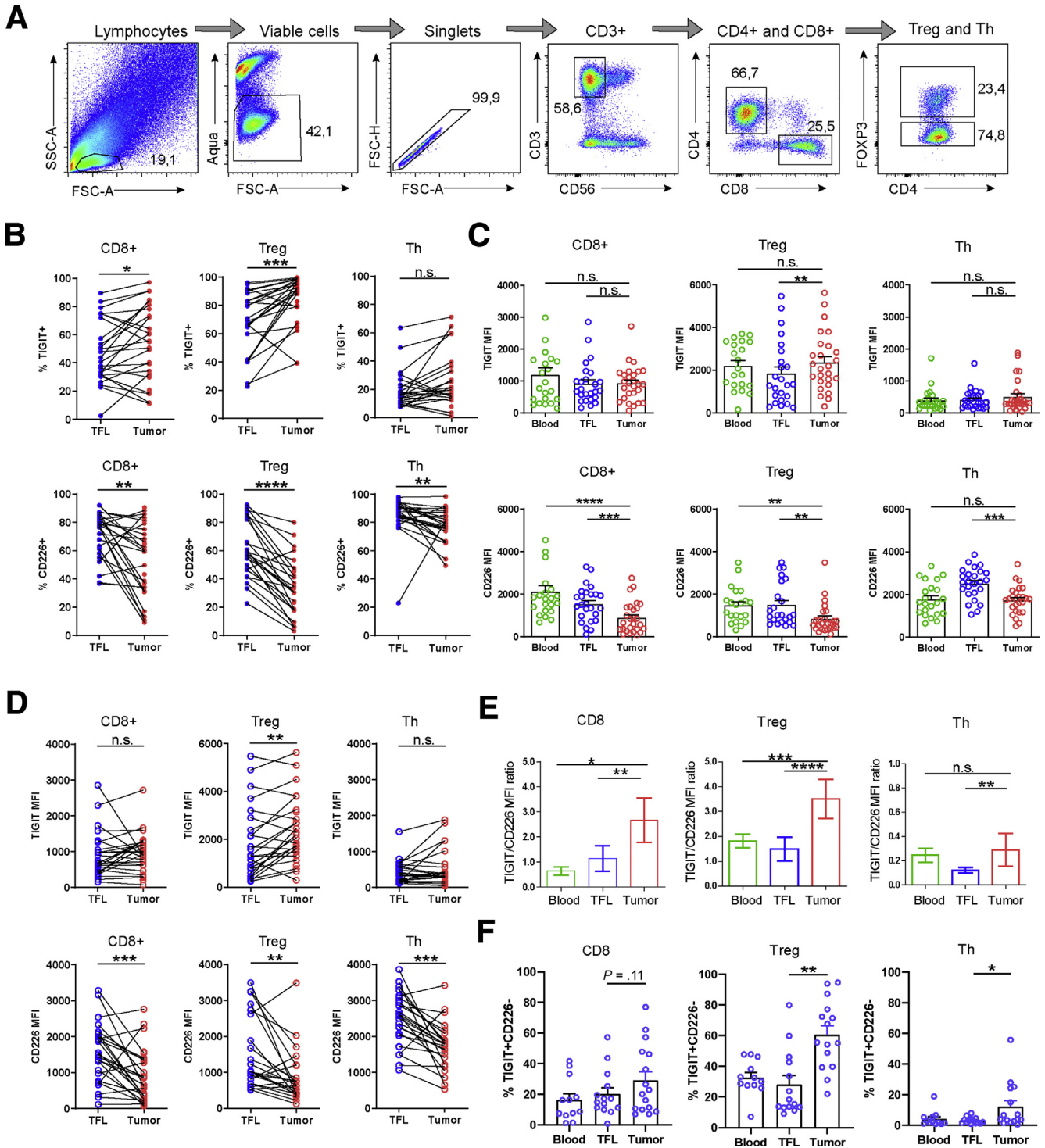
Most current article

Figure 1. TIGIT/CD226 MFI ratio is increased on intratumoral Treg and CD8$^+$ T cells. (*A*) Gating strategy of CD8, Treg, and Th. (*B*) Frequencies of TIGIT$^+$ and CD226$^+$ cells in T-cell subsets in tumor and TFL of individual patients are shown. (*C* and *D*) MFIs of TIGIT and CD226 on CD8$^+$ T, Treg, and Th cells in blood, TFL, and tumor (n = 28). (*E*) MFI ratio of TIGIT/CD226 in CD8$^+$ T, Treg, and Th cells. (*F*) Frequency of TIGIT$^+$CD226$^-$ subset in CD8, Treg, and Th in blood, TFL, and tumor (n = 16). *$P <$ .05, **$P <$ .01, ***$P <$ 0001. *Dots* represent individual patients. *Bars* represent mean $\pm$ standard error of the mean (SEM).

TIGIT Is Enriched and CD226 Is Down-regulated on Intratumoral PD1^{high} CD8$^+$ TILs

Consistent with Kim et al[26] and Ma et al,[27] we observed 2 subgroups of HCC patients that were based on the presence or absence of a distinct PD1^{high} subpopulation in tumor-derived CD8$^+$ T cells. HCC patients with a PD1^{high} CD8$^+$ TILs population were termed high PD1 expressers (Figure 3A, Figure 4A), whereas patients with only PD1-intermediate CD8$^+$ TILs were called low PD1 expressers

(Figure 3A, Figure 4B). High PD1 expressers comprised 68% of the total analyzed population (Figure 3A). All tumor-derived PD1^{high} CD8$^+$ T cells expressed TIGIT (Figure 3B). The PD1^{high} TIGIT$^+$ fraction comprised on average 58% of the total CD8$^+$ TILs, and part of these cells co-expressed the co-inhibitory receptors TIM3 and LAG3 (Figure 3B, Figure 4C). Interestingly, in contrast to TIM3 and LAG3, TIGIT was also expressed on a subset of CD8$^+$ PD1^{int} TILs in high PD1 expressers (Figure 3B). Moreover, this subset showed higher expression of CD226 than PD1^{high} CD8$^+$ TILs (Figure 3B). High PD1 expressers had significantly increased frequencies of TIGIT-expressing CD8$^+$ TILs, but in low PD1 expressers percentages of CD226-expressing CD8$^+$ TILs were enhanced. MFIs of TIGIT and CD226 showed the same differences (Figure 3C). In high PD1 expressers, ratios of TIGIT/CD226 on CD8$^+$ T cells were up-regulated in tumor compared with TFLs and blood (Figure 3D) and correlated positively with the frequencies of PD1^{high} CD8$^+$ TILs (Figure 4D). In low PD1 expressers, ratios of TIGIT/CD226 on CD8$^+$ T cells did not differ between tumor, TFLs, and blood (Figure 4E). Within high PD1 expressers, both the frequencies and MFIs of TIGIT increased stepwise according to the level of PD1 expression on CD8$^+$ T cells (Figure 3E), whereas CD226 frequency and MFI were negatively associated with PD1 expression (Figure 3F). Consequently, the ratio of TIGIT/CD226 was strongly enhanced in tumor-infiltrating PD1^{high} CD8$^+$ T cells but only minimally on PD1^{int}CD8$^+$ compared with PD1$^-$ CD8$^+$ TILs (Figure 3G). In low PD1 expressers, TIGIT expression was minimally increased in PD1^{int} CD8$^+$ compared with PD1$^-$ CD8$^+$ TILs (Figure 3H), whereas CD226 did not show any difference (Figure 3I). The ratios of TIGIT/CD226 on PD1^{int} and PD1- CD8$^+$ TILs in low PD1 expressers were all smaller than 1 (Figure 3J). Nevertheless, the PD1^{int} TIGIT$^+$ fraction of total CD8$^+$ TILs in low PD1 expressers was larger than in high PD1 expressers (on average 37% of total CD8$^+$ TILs [Figure 4F] versus 14% [Figure 3B]), respectively. The frequencies of PD1^{high} CD8$^+$, TIGIT$^+$ CD8$^+$ T cells, and the ratios of TIGIT/CD226 on CD8$^+$ TILs correlated positively with serum alpha-fetoprotein (AFP) concentrations in individual patients (Figure 4G–I).

Collectively, in high PD1 expressers TIGIT expression correlated with PD1 expression, and TIGIT/CD226 ratios were maximally increased on PD1^{high} CD8$^+$ TILs, whereas in low PD1 expressers CD8$^+$ TILs contain a larger proportion of PD1^{int} cells with TIGIT/CD226 ratios smaller than 1.

PD1^{high} TIGIT$^+$ CD8$^+$ TILs Are Functionally Exhausted With High Thymocyte Selection-Associated High Mobility Group Box Protein Expression

Thymocyte selection-associated high mobility group box protein (TOX) has been identified as a major driver of epigenetic changes associated with CD8+ T-cell exhaustion and has a role in maintaining survival of exhausted T cells.[28–30] A transcription factor T cell factor 1 (TCF1)$^+$ stem cell–like progenitor population exists with exhausted CD8$^+$

TILs that might be responsible for the proliferative and functional responses that occur after immune checkpoint blockade.[31–33] We therefore examined TOX and TCF1 expression in the different CD8$^+$ TIL subsets. In high PD1 expressers, the expression of TOX was specifically up-regulated in PD1^{high} TIGIT$^+$ CD8$^+$ TILs, whereas TCF1 expression was down-regulated in this subset (Figure 5A–C). PD1^{high} TIGIT$^+$ CD8$^+$ TILs also expressed higher levels of activation markers Ki67, CD38, and HLA-DR (Figure 5D–F). Co-expression of CD39 and CD103 identifies tumor-reactive CD8$^+$ T cells in multiple human solid tumors.[34] Here we found a higher frequency of CD39$^+$CD103$^+$ cells in PD1^{high} TIGIT$^+$ CD8$^+$ TIL subset compared with other subsets (Figure 5G).

Because dysfunctional production of cytotoxins is a feature of exhaustion, we analyzed their intracellular expression directly ex vivo. The expression of granzyme B and perforin was significantly reduced in the PD1^{high} TIGIT$^+$ fraction compared with PD1^{int} TIGIT$^+$ fraction (Figure 5H). Interestingly, the PD1^{int} TIGIT$^+$ CD8 TIL subset tended to contain the most cytotoxins (Figure 5H). Furthermore, we stimulated TILs with phorbol 12-myristate 13-acetate (PMA) and ionomycin to assess effector cytokine production by flow cytometry. The percentages of tumor necrosis factor (TNF)-α– and IFN-γ–producing cells were lowest in PD1^{high} TIGIT$^+$ cells compared with the other CD8$^+$ TIL fractions (Figure 5I).

PD1^{high} TIGIT$^+$ CD8$^+$ T cells were also present in TFLs of high PD1 expressers (Figure 6A), and part of these cells expressed TIM3 but not LAG3 (Figure 6B and C). However, although this subset showed a decreased TCF1 level, it did not up-regulate TOX (Figure 6D and E). Notably, CD226 was not down-regulated, and the ratios of TIGIT/CD226 were only modestly increased in PD1^{high} CD8$^+$ T cells in TFLs (Figure 6F–H) compared with those ratios on PD1^{high} CD8$^+$ TILs (Figure 3H). The expression of perforin but not granzyme B was significantly reduced in the PD1^{high} TIGIT$^+$ fraction compared with PD1^{int} TIGIT$^+$ fraction in TFLs (Figure 6I).

These data demonstrate that in contrast to PD1^{int} CD8$^+$ TILs, PD1^{high} TIGIT$^+$ CD8$^+$ TILs are highly activated, terminally differentiated dysfunctional T cells that are characterized by high TOX expression.

CD155 Is Present on Tumor-Infiltrating Antigen-Presenting Cells and Overexpressed on HCC Tumor Cells

Because CD155 is the high affinity ligand for TIGIT and CD226, we analyzed CD155 expression on antigen-presenting cell (APC) subsets in tumors. We focused on 3 major APC subsets, CD45$^+$ BDCA1$^+$ CD19$^-$ conventional dendritic cells (cDC), CD45$^+$ CD14$^+$ monocytes/macrophages, and CD45$^+$ CD19$^+$ B cells (Figure 7A). The percentages of cDC, monocytes/macrophages, and B cells in tumor tissues did not significantly differ from those in TFLs (Figure 8A). Prominent expression of CD155 was found on cDC and monocytes and low expression on B cells (Figure 7B, Figure 8B and C). Both frequencies and MFI of CD155 expression on APCs in tumor did not differ with that in TFLs and blood. We also examined CD155 protein
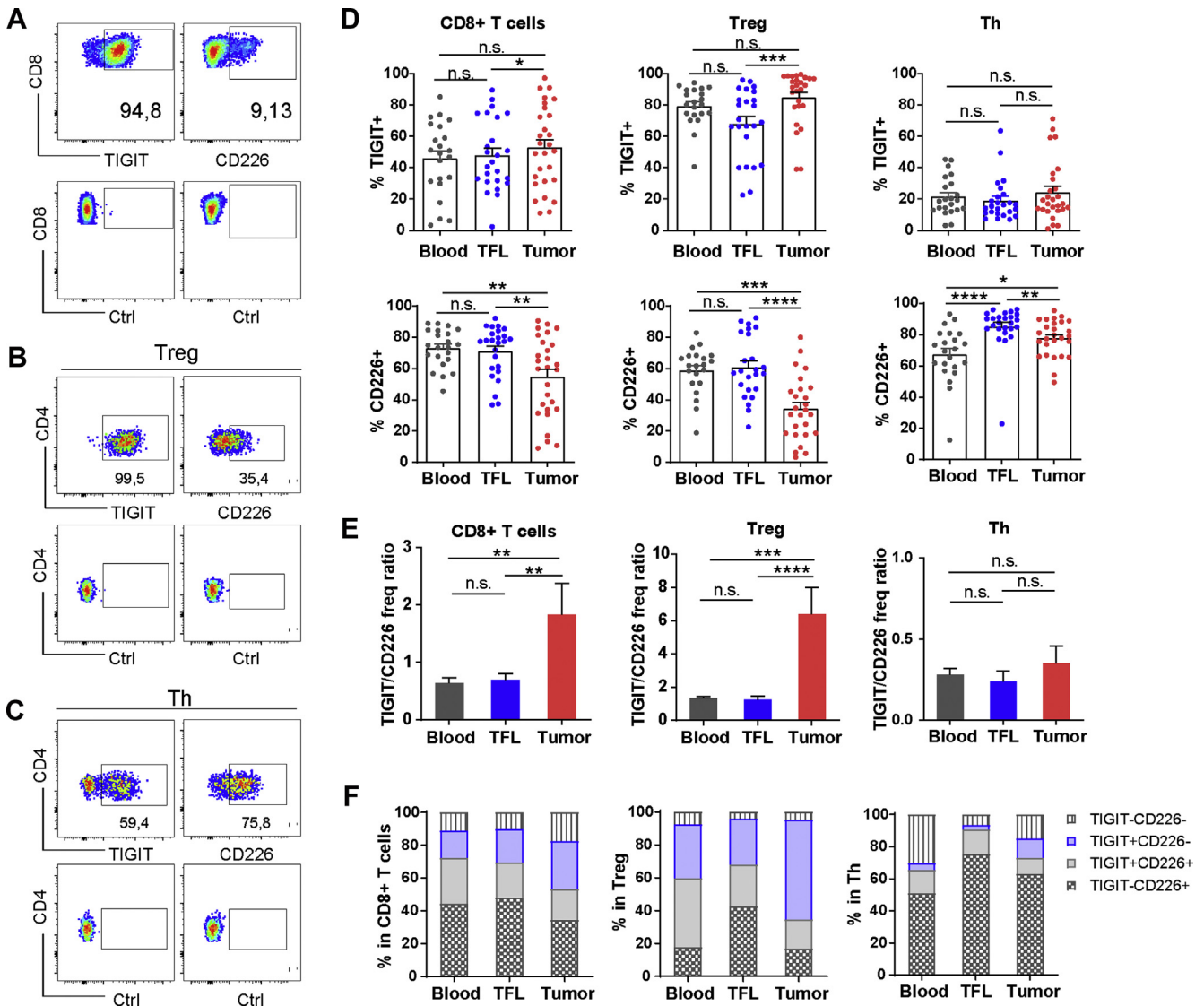
Figure 2. TIGIT/CD226 ratio is increased on intratumoral Treg and CD8$^+$ T cells. (A–C) Flow cytometry plots of TIGIT and CD226 expression on tumor-infiltrating CD8$^+$ T, Treg, and Th cells. (D) Percentages of TIGIT and CD226 positive cells among CD8$^+$ T, Treg, and Th cells in blood, TFL, and tumor (n = 28). (E) Frequency ratio of TIGIT/CD226 in CD8$^+$ T, Treg, and Th cells. (F) Mean percentage of co-expression of TIGIT and CD226 among CD8$^+$ T, Treg, and Th cells in tumors, TFLs, and blood from HCC patients (n = 16). *Dots* represent individual patients. *Bars* represent means ± SEM. *$P < .05$, **$P < .01$, ***$P < .001$.

expression on tumor cells using tissue microarrays (TMAs) with cores of tumors and TFLs from 97 HCC patients by immunohistochemistry.[35,36] We found that most tumor cells express CD155 and that expression was significantly up-regulated on tumor cells compared with hepatocytes in TFLs (Figure 8D and E).

These data demonstrate that CD155 is highly expressed in the tumor microenvironment, suggesting that TIGIT$^+$ TILs interact with CD155$^+$ cells within the tumor, which might result in T-cell inhibition.

Combined TIGIT and PD1 Blockade Enhances ex vivo Functionality of CD8$^+$ TILs

We tested whether co-blocking TIGIT and PD1 can improve functionality of tumor-infiltrating T cells. We

isolated on average 2.74×10^6 CD45$^+$ leukocytes per gram of tumor (Figure 9A and B). We stimulated TILs with a suboptimal amount of anti-CD3/CD28 beads in the presence or absence of mouse anti-human TIGIT (10 μg/mL) and/or anti-PD1 (nivolumab, 10 μg/mL), which completely blocked TIGIT and PD1 on CD8$^+$ TILs until the end of the cultures (Figure 9C), or isotype-matched control antibodies. After 4 days, T-cell proliferation (Figure 9D) and cytokine production were measured by flow cytometry. Single nivolumab treatment resulted in a minor increase in CD8$^+$ TIL proliferation (Figure 10A), whereas single TIGIT blockade did not (Figure 9E). But co-blockade of TIGIT and PD1 significantly enhanced the proliferation of CD8$^+$ TILs compared with single PD1 blockade (Figure 10A). The stimulatory effect of co-blockade compared with single PD1 blockade was mainly observed in low PD1 expressers and not observed in high

PD1 expressers (Figure 10B). A higher concentration of TIGIT blocking antibody (20 μg/mL) in combination with nivolumab did not have added value to reinvigorate CD8$^+$

TIL proliferation in high PD1 expressers (Figure 9F). Combined blockade of TIGIT and PD1 also enhanced ex vivo proliferative responses of CD8$^+$ TILs of HCC patients to
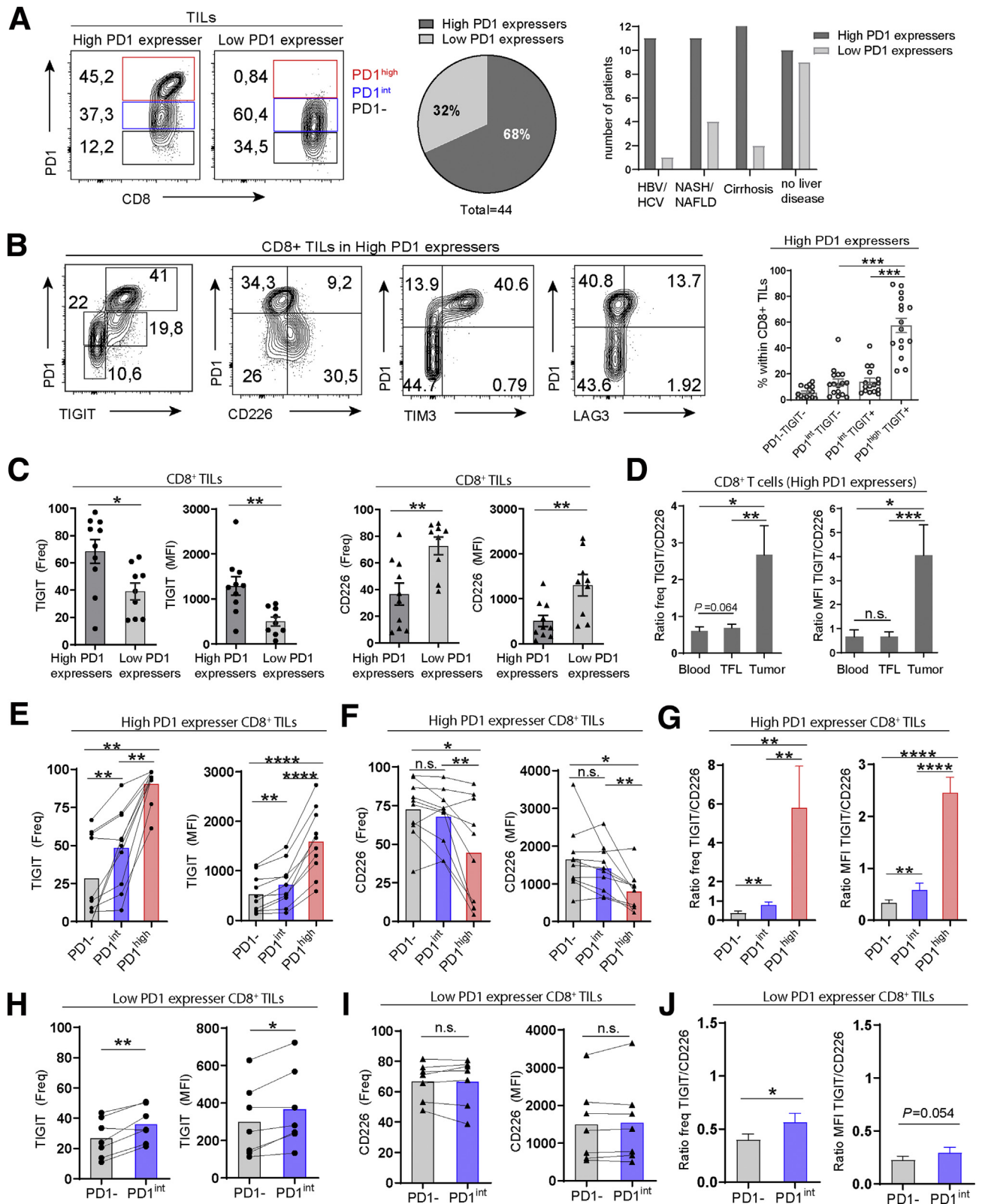
tumor antigens GPC3 and/or MAGEC2 presented by autologous B cells (Figure 9G and H, Figure 10C).

To compare the survival and proliferative ability of PD1^{high} and PD1^{int} and PD1$^-$ CD8$^+$ TILs, from high PD1 expressers we sorted PD1^{high} CD8$^+$ and PD1^{int} plus PD1$^-$ CD8$^+$ TILs and cultured each of those populations together with the remaining CD45$^+$ CD8$^-$ TILs in the presence of anti-CD3/CD28 beads. PD1^{high} CD8$^+$ T cells showed limited expansion capacity compared with the PD1^{int} and PD1$^-$ subsets (Figure 10D).

In addition, compared with single PD1 blockade, co-blockade of TIGIT/PD1 significantly enhanced IFN-γ production in CD8$^+$ TILs of low PD1 expressers (Figure 10E and F) and also in CD8$^+$ TILs from some high PD1 expressers. Moreover, we used an HCC cell line (HepG2) to evaluate the effect of co-blockade on cytotoxicity of anti-CD3/CD28–stimulated purified CD3$^+$ TILs. Because HepG2 cells expressed high levels of CD155 but low levels of PD-L1, we induced PD-L1 expression on HepG2 by IFN-γ pre-treatment for 48 hours (Figure 11A). CD155 expression did not change after IFN-γ treatment (Figure 11B). Combined PD1/TIGIT antibody blockade significantly enhanced cyto-toxicity of CD3$^+$ TILs against HepG2 compared with single PD1 blockade (Figure 10G, Figure 11C).

Collectively, these data demonstrate that compared with anti-PD1 monotherapy, co-blockade of TIGIT with PD1 improves ex vivo CD8$^+$ TIL proliferation, IFN-γ production, and cytotoxicity as well as reactivity of CD8$^+$ TILs against tumor antigens.

Combined TIGIT and PD1 Blockade Enhances ex vivo Functionality of CD8$^+$ TILs not Responding to Anti-PD1 Single Blockade

We next asked 2 questions: (1) whether combined blockade of TIGIT/PD1 can convert anti-PD1 non-responders to responders, and (2) whether co-blockade can further enhance CD8$^+$ TIL function in anti-PD1 responders. We stratified HCC patient TILs into nivolumab responders (11/22, 50%) and non-responders (11/22, 50%) on the basis of CD8$^+$ TIL proliferation on ex vivo single PD1 blockade (Figure 12A). Strikingly, compared with only blocking PD1, co-blockade of TIGIT/PD1 significantly enhanced the proliferation of CD8$^+$ TILs in nivolumab non-responders but not in nivolumab responders (Figure 12B). Similarly, nivolumab/anti-TIGIT treatment significantly improved IFN-γ production by CD8$^+$ TILs from nivolumab non-responders, although also enhanced IFN-γ production

was observed in CD8$^+$ TILs of some nivolumab responders (Figure 12C). However, enhanced TIL cytotoxicity against HepG2 was observed in both groups on co-blockade (Figure 12D). Interestingly, 73% of nivolumab responders were high PD1 expressers (Figure 12F), suggesting that high PD1 expressers tend to respond better to PD1 blockade.

CD226 Is Required for the Effect of TIGIT Blockade

Because CD226 is the co-stimulatory counterpart of TIGIT, we assessed whether CD226 expression is affected by TIGIT blockade and whether CD226 is required for the stimulatory effects of TIGIT blockade that we observed in TIL cultures of some patients. In ex vivo polyclonal assays, we observed that TIGIT blockade significantly up-regulated both CD226^{hi} frequencies and CD226 MFIs on day 4 (Figure 13A and B). Furthermore, the percentages of CD226^{hi} CD8$^+$ TILs correlated with the frequencies of Ki67$^+$CD8$^+$ TILs after TILs were used in ex vivo polyclonal assays with or without anti-TIGIT or dual blocking antibodies (Figure 13C). Notably, the addition of anti-CD226 blocking antibodies to TILs that responded to single TIGIT blockade abrogated the effect of TIGIT blockade partially (Figure 13D and E).

Taken together, CD226 expression can be up-regulated by TIGIT blockade and is partially required for the stimulatory effects of TIGIT blockade on CD8$^+$ TILs.

Discussion

The aims of this study were to characterize TIGIT-expressing TILs in HCC patients and to determine whether co-blockade of TIGIT and PD1 has added value over PD1 single blockade to restore functionality of HCC TILs. We observed elevated ratios of TIGIT/CD226 expression on intratumoral CD8$^+$ T cells and Treg compared with their counterparts in TFLs and blood. This allows more frequent interaction of TIGIT on these TIL subsets with its high affinity ligand CD155 expressed on APCs or tumor cells. This interaction may have different effects on CD8$^+$ T cells and Treg. In CD8$^+$ T cells, TIGIT signaling can directly or indirectly inhibit their cytotoxic/effector function[18,20]; in Treg, TIGIT signaling can directly promote their suppressive functions,[25,37] or Treg can induce interleukin 10 production by dendritic cells via TIGIT signaling, which also results in suppression of anti-tumor effector T-cell responses.[12]

Figure 3. (*See previous page*). **TIGIT is enriched and CD226 is down-regulated on intratumoral PD1^{high} CD8$^+$ T cells.** (*A*) Flow cytometry plots revealed stratification of HCC patients on the basis of differential PD1 expression on tumor-infiltrating CD8$^+$ T cells. The gate to define the PD1^{high} subsets was set on the basis of the intermediate PD1 expression of CD8$^+$ TILs. The percentage of high PD1 expresser and its association with etiology are shown (n = 44). (*B*) Flow cytometry plots of co-expression of PD1 and TIGIT, CD226, TIM3, and LAG3 in high PD1 expressers. Percentages of co-expression of TIGIT and PD1 are shown (n = 16). (*C*) Expression of TIGIT and CD226 on CD8$^+$ TILs in high or low PD1 expressers. (*D*) Ratios of TIGIT/CD226 in blood, TFL, and tumor. (*E* and *F*) Expression of TIGIT and CD226 in the PD1$^-$, PD1^{int}, and PD1^{high} subsets of CD8$^+$ TILs in high PD1 expressers (n = 10). (*G*) Ratios of TIGIT/CD226 in PD1$^-$, PD1^{int}, and PD1^{high} subsets of CD8$^+$ TILs high PD1 expressers (n = 10). (*H* and *I*) Expression of TIGIT and CD226 in the PD1$^-$ and PD1^{int} subsets of CD8$^+$ TILs in high PD1 expressers (n = 7). (*J*) Ratios of TIGIT/CD226 in PD1$^-$ and PD1^{int} subsets of CD8$^+$ TILs in low PD1 expressers (n = 7). *Dots* represent individual patients. *Bars* show mean or mean ± SEM.

Kim et al[26] and Ma et al[27] have shown that PD1 is differentially expressed on CD8$^+$ TILs in about half of HCC patients, and that PD1^{high} CD8$^+$ TILs are functionally

the most exhausted subpopulation. Wang et al[38] have shown that TOX is up-regulated in functionally exhausted PD1^{high} CD8$^+$ TILs in HCC. Here, we confirmed these
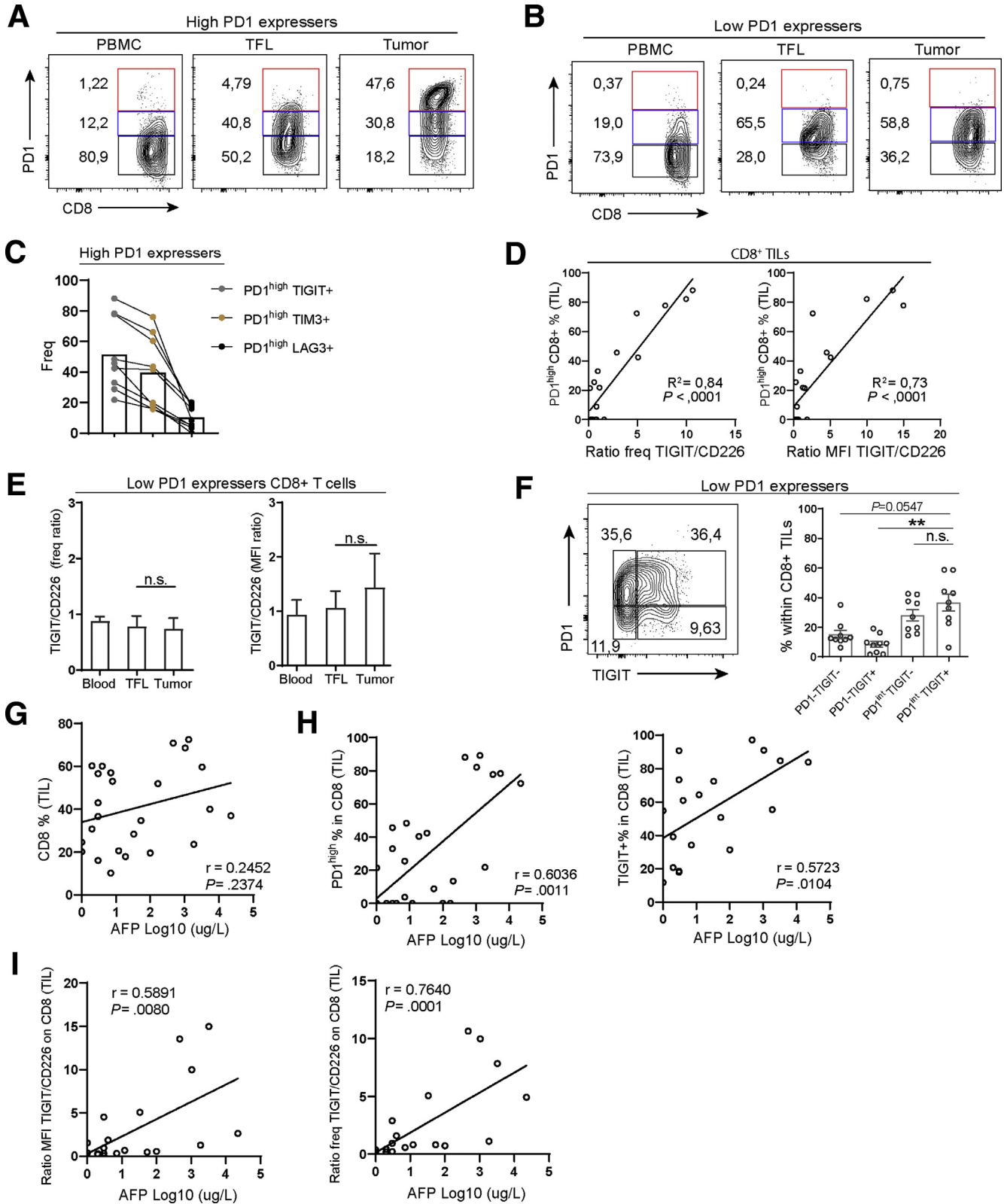
observations, and we extended them by showing that the PD1^{high} CD8^{+} TIL subset has the lowest expression of the cytotoxins granzyme B and perforin and co-expresses CD39 and CD103, suggesting enrichment with tumor-specific T cells. We further demonstrated that TIGIT expression was enriched whereas CD226 expression was down-regulated on PD1^{high} CD8^{+} TILs compared with CD8^{+} PD1^{int} and CD8^{+}PD1^{-} TILs. Consequently, PD1^{high} TIGIT^{+} CD8^{+} TILs had the highest TIGIT/CD226 ratios compared with other CD8^{+} subsets. Because a large part of these cells also expressed the co-inhibitory receptors TIM3 and/or LAG3, our data suggest that the PD1^{high} TIGIT^{+} subset represents the terminally differentiated and exhausted CD8^{+} TIL subset in HCC tumors. In agreement with Kim et al,[26] we found that high PD1 expressers were mainly found among patients with high serum AFP levels. Ma et al[27] reported recently that the presence of CD8^{+} PD1^{hi} T cells in HCC tumors is associated with poor prognosis, and Liu et al[39] found that elevated levels of peripheral PD1^{+} TIGIT^{+} CD8^{+} T cells are associated with poor prognosis of patients with hepatitis B virus–related HCC.

Interestingly, we demonstrate that the more PD1^{high} TIGIT^{+} CD8^{+} T cells in tumor, the more PD1^{high} TIGIT^{+} CD8^{+} T cells were found in TFLs. PD1^{high} TIGIT^{+} CD8^{+} T cells in TFLs did not show increased levels of TOX, and neither reduced CD226 and granzyme B expression. Apparently, PD1^{high} TIGIT^{+} CD8^{+} T cells in the tumors are in a further stage of exhaustion than their counterparts in TFL. This may be caused by chronic T-cell receptor stimulation in the tumor microenvironment. Several studies have shown that TOX expression was increased and remained high in exhausted CD8^{+} T cells by chronic T-cell receptor stimulation, whereas only low-level and transient TOX up-regulation was seen in CD8^{+} T cells during acute infection.[28–30] TOX expression in CD8^{+} TILs may be further supported by tumor-derived factors, such as vascular endothelial growth factor-A, that drive exhaustion in CD8^{+} TILs.[40] Further research is required to understand the specific factors in HCC tumor microenvironment that increase TOX levels on PD1^{high} CD8^{+} TILs.

We performed polyclonal and tumor antigen–specific functional assays to test the effects of blocking PD1 and TIGIT on tumor-infiltrating CD8^{+} TILs ex vivo. Compared with single PD1 blockade, co-blockade of TIGIT/PD1 increased IFN-γ production by CD8^{+} TILs of some high PD1 expressers but did not improve their proliferation. This might be caused by limited survival

capacity and a terminally differentiated and exhausted state of CD8^{+} TILs. In contrast, CD8^{+} TILs of low PD1 expressers exhibited enhanced proliferation and cytokine production in response to co-blockade. CD8^{+} TILs of these patients are not terminally differentiated and also express more CD226, thereby allowing better co-stimulation on TIGIT blockade. Another hypothesis is that the PD1^{int} TIGIT^{+} CD8^{+} subset, which was enriched in low PD1 expressers, may mediate the enhanced proliferative response. On average, 60% of PD1^{int} TIGIT^{+} CD8^{+} TILs expressed TCF1. TCF1 is a key transcription factor of progenitor exhausted CD8^{+} T cells, which express intermediate PD1, to produce differentiated effector T-cell progeny and to maintain themselves.[31,32] This PD1^{int} progenitor exhausted CD8^{+} T-cell subset mediates responses to PD1 checkpoint pathway blockade. Accordingly, PD1^{int} TIGIT^{+} CD8^{+} TILs may be expanded after TIGIT/PD1 blockade to fill up the effector-type pool. Further work is required to unravel the role of these PD1^{int} TIGIT^{+} TCF1^{+} CD8^{+} T cells in response to checkpoint blockade in HCC patients.

In HCC, the question still remains how to improve the response rate to anti-PD1 therapy. Here we found TIGIT/PD1 co-blockade could improve ex vivo proliferation, cytokine production, and cytotoxicity of CD8^{+} TILs that did not respond to nivolumab ex vivo. Interestingly, CD8^{+} TILs that ex vivo responded to single PD1 blockade were mainly derived from high PD1 expressers (Figure 12E). In contrast, the vast majority of combination-blockade responding CD8^{+} TILs were derived from low PD1 expressers (Figure 10B, 78% and Figure 12B, 73%), suggesting that especially tumors with intermediate (and not high) PD1 expressing CD8^{+} TILs may display improved benefit from combined treatment with anti-PD1 and anti-TIGIT.

CD226 deficiency has been shown to impair antitumor T-cell effector function.[41] Here we found that blocking TIGIT up-regulated CD226 on CD3/CD28-stimulated CD8^{+} TILs, which enabled CD226 to interact more frequently with CD155. The linear correlation between CD226 and Ki67 expression after culture indicates the enhanced expression of CD226 might be responsible for the increased proliferation of CD8^{+} TILs. TIGIT may act directly to compete with CD226 for ligand binding.[12,19] Johnston et al[20] showed that TIGIT directly interacts with CD226 and that this interaction impairs CD226 homodimerization and function. Here we showed neutralizing CD226 on CD8^{+} TILs can counteract the effect of TIGIT blockade.

Figure 4. (*See previous page*). TIGIT/CD226 ratios are not up-regulated on intratumoral CD8^{+} T cells from low PD1 expressers. (*A* and *B*) Gating strategy of PD1^{high}, PD1^{int}, and PD1^{-} in tumor, TFL, and blood in high and low PD1 expressers. (*C*) Percentages of PD1^{high} TIGIT^{+}, PD1^{high} TIM3^{+}, and PD1^{high} LAG3^{+} in CD8^{+} TILs from high PD1 expressers. *Bars* show means. (*D*) Correlation of PD1^{high} CD8^{+} TIL with frequency and MFI ratios of TIGIT/CD226 in CD8^{+} TILs (n = 19). (*E*) Ratios of TIGIT/CD226 in CD8^{+} T cells in blood, TFL, and tumor from low PD1 expressers. *Bars* show mean ± SEM (n = 10). (*F*) Co-expression of TIGIT and PD1 on CD8^{+} TILs from low PD1 expressers (n = 9). (*G*) Correlation between CD8^{+} TIL frequency and serum AFP level from HCC patients. (*H*) Correlation between PD1^{high} CD8^{+} TIL frequency and serum AFP level, TIGIT^{+}CD8^{+} TIL frequency and serum AFP level from HCC patients. (*I*) Correlation between MFI or frequency ratios of TIGIT/CD226 and serum AFP level from HCC patients. *P < .05, **P < .01, ***P < .001. PBMC, peripheral blood mononuclear cells.
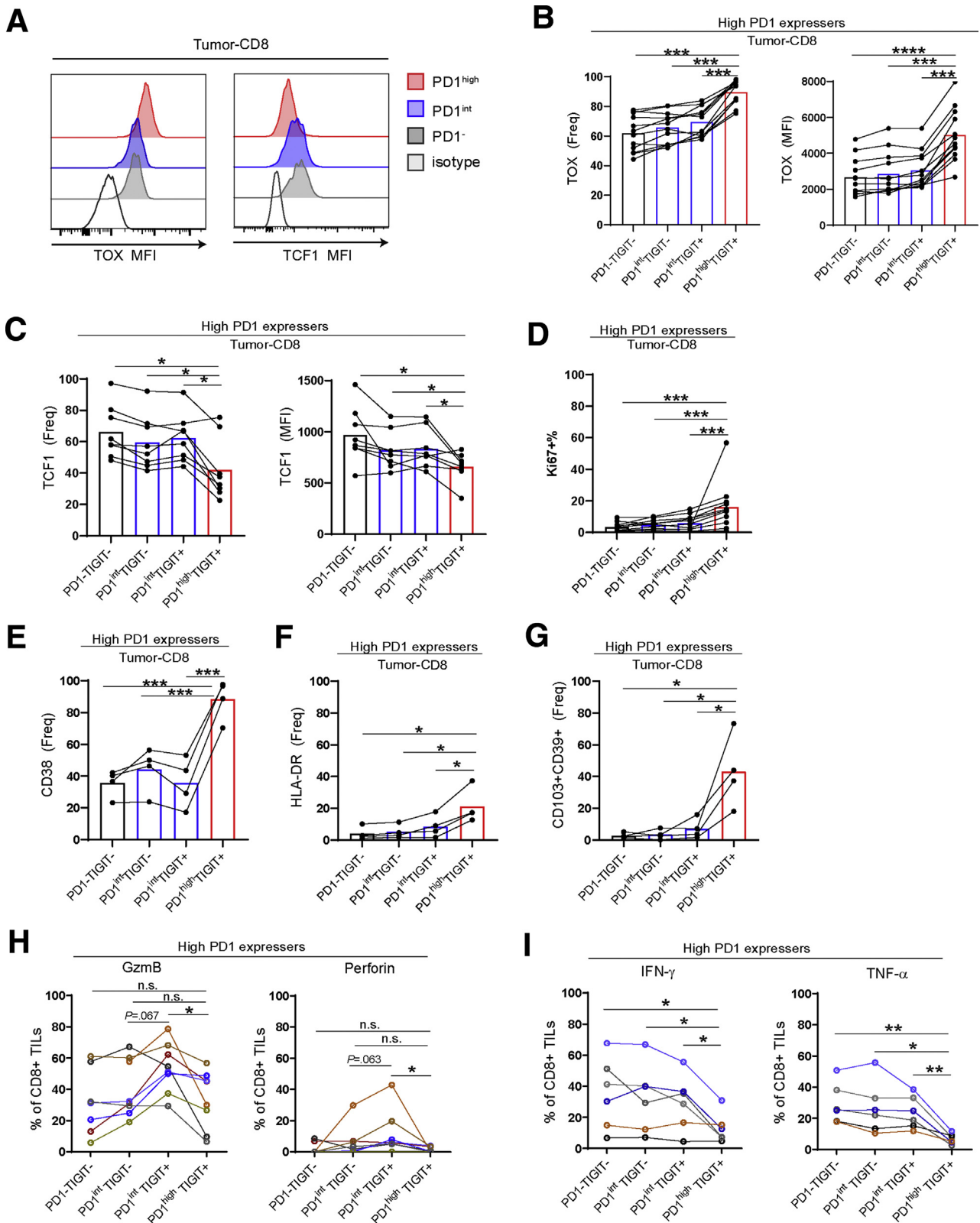
Figure 5. PD1^{high} TIGIT⁺ CD8⁺ TILs are functionally exhausted with high TOX expression. (*A*) Flow cytometry plots of TOX and TCF1 expression in PD1⁻, PD1^{int}, and PD1^{high} CD8⁺ TILs. (*B–F*) Expression of TOX, TCF1, Ki67, CD38, and HLA-DR in 4 subsets of CD8⁺ TILs in high PD1 expressers. *Dots* represent individual patients, and *bars* show mean. (*G*) Co-expression of CD39 and CD103 in 4 subsets of CD8⁺ TILs in high PD1 expressers. (*H*) Percentages of intracellular granzyme B and perforin expression in 4 subsets of CD8⁺ TILs in high PD1 expressers. (*I*) Production of IFN-γ and TNF-α by 4 subsets of CD8⁺ TILs in high PD1 expressers after PMA/ionomycin stimulation. *$P < .05$, **$P < .01$, ***$P < .001$. GzmB, granzyme B.
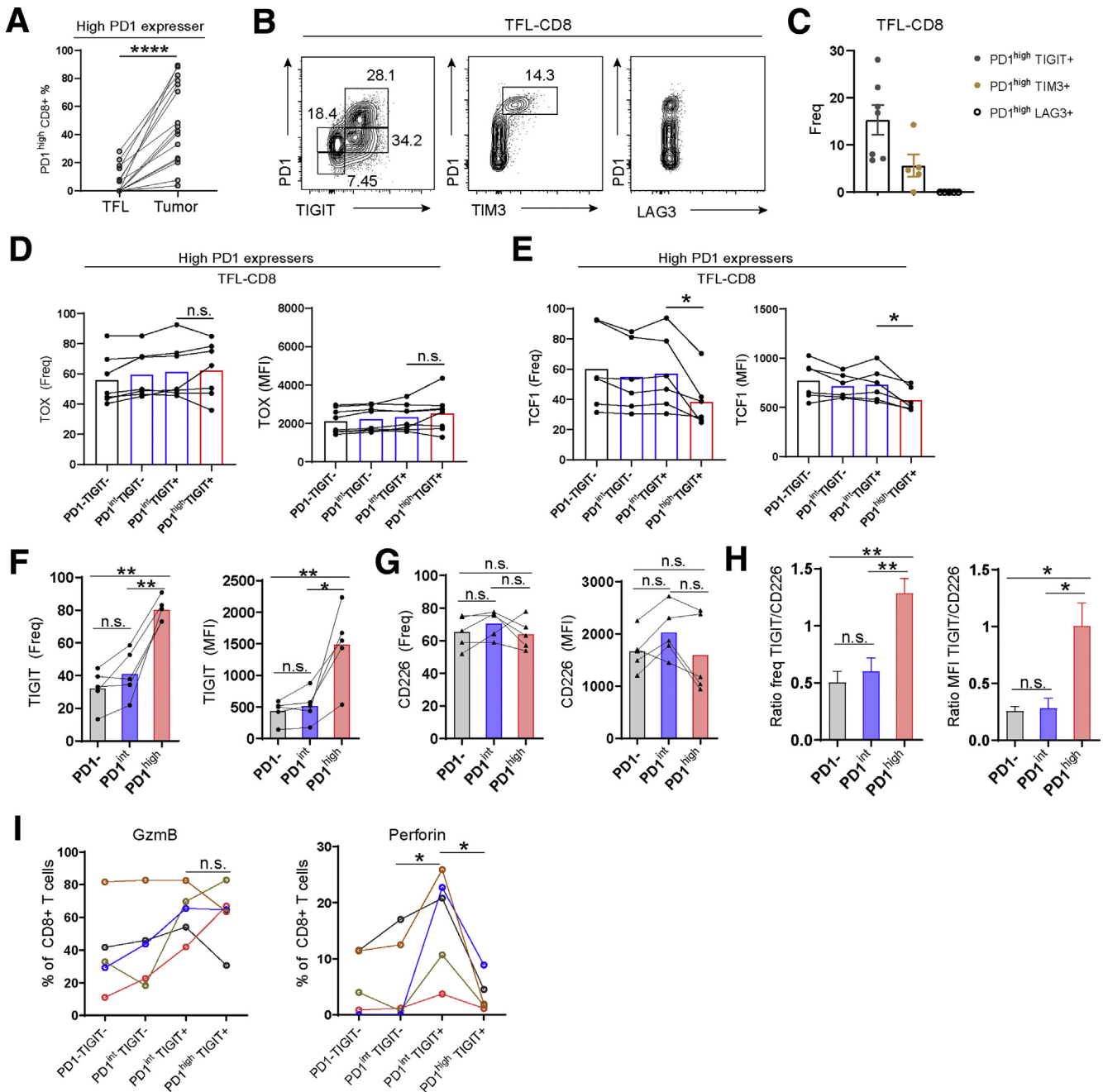
Figure 6. PD1^high TIGIT+ CD8+ T cells were also present in TFLs of high PD1 expressers. (*A*) Frequencies of PD1^high CD8+ T cells in TFL and tumor from high PD1 expressers (n = 16). (*B*) Fluorescence-activated cell sorter plots show co-expression of PD1 and TIGIT, TIM3, and LAG3 on CD8+ T cells in TFLs containing PD1^high CD8+ T cells. (*C*) Frequencies of PD1^high TIGIT+, PD1^high TIM3+, and PD1^high LAG3+ within CD8+ T cells in TFLs. (*D and E*) Expression of TOX and TCF1 in 4 subsets of CD8+ T cells in TFLs. (*F and G*) Expression of TIGIT and CD226 in the PD1⁻, PD1^int, and PD1^high subsets of CD8+ T cells in TFLs (n = 5). *Dots* represent individual patients, and *bars* show mean. (*H*) Ratios of TIGIT/CD226 in PD1⁻, PD1^int, and PD1^high subsets of CD8+ T cells in TFLs. *Bars* show mean ± SEM. (*I*) Percentages of intracellular granzyme B (GzmB) and perforin expression in 4 subsets of CD8+ T cells in TFLs. *P < .05, **P < .01.

CD155 is the shared ligand for TIGIT and CD226. We found that CD155 is abundant on APCs (cDC and mono-cytes) and present on HCC tumor and TFLs. We also found that the CD155 protein level was up-regulated in HCC tumors compared with TFLs. Duan et al[42] found that mRNA and protein levels of CD155 were higher in HCC cancer tissues than those in adjacent tumor-free tissues. The expression of CD155 gradually decreased as differentiation increased. Sun et al[43] showed that higher intratumoral CD155 expression is correlated to a poorer prognosis of HCC patients. The high expression of CD155 can contribute to the suppression of immune responses if
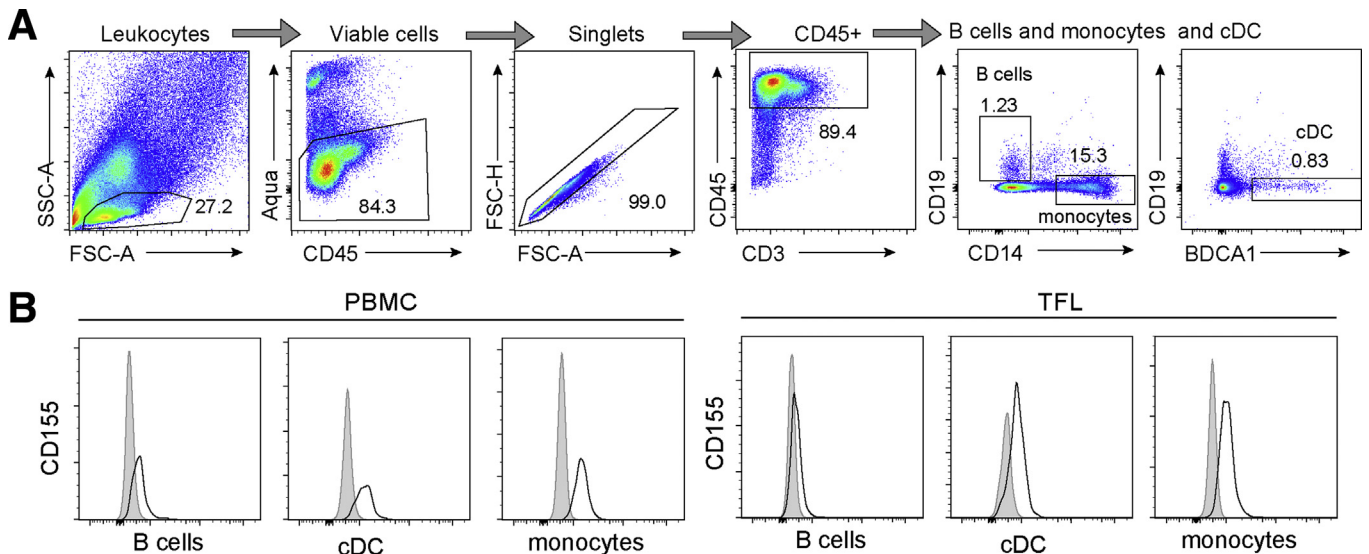
Figure 7. Gating strategy of APCs. (*A*) Gating strategy of CD19$^+$ B cells, CD14$^+$ monocytes, and CD19$^-$ BDCA1$^+$ cDC is shown. (*B*) Representative flow cytometry plots of CD155 expression on B cells, cDC, and monocytes in peripheral blood mononuclear cells and TFLs.

TIGIT/CD226 ratios are elevated in the tumor microenvironment.

Our study has a few limitations. (1) Checkpoint therapy is currently used to treat advanced HCC patients. However, the HCC cohort in this study is a representative cohort for resectable/early stage HCC patients in Western countries. (2) Considering the predominant expression of TIGIT and increased TIGIT/CD226 ratios on tumor-infiltrating Treg, Treg may be involved in the observed effects of co-blockade. However, after depletion of CD4$^+$ CD25$^+$ Treg by magnetic sorting, combination treatment still enhanced CD8$^+$ TIL proliferation and IFN-γ production (data not shown), suggesting that T cells (non-Treg) are direct targets for co-blockade; further research is needed to unravel the role of TIGIT on Treg functions in HCC in more detail.

In summary, we conclude that TIGIT is enriched in PD1^{high} CD8$^+$ TILs, and this subset represents the most dysfunctional and exhausted CD8$^+$ TIL fraction. Unlike TIM3 and LAG3, TIGIT is also expressed on the PD1^{int} CD8$^+$ subset that co-expresses CD226 and is prominent in tumors of HCC patients that do not have CD8$^+$PD1^{high} TILs. CD8$^+$ TILs of these patients preferentially respond ex vivo to dual TIGIT/PD1 blockade. Compared with single PD1 blockade, co-blockade of TIGIT/PD1 improved CD8$^+$ TIL cytotoxicity and converted CD8$^+$ TILs that ex vivo did not respond to PD1 blockade to responders. Therefore, co-blocking TIGIT and PD1 could be a promising immune therapeutic strategy for HCC patients. The clinical proof of efficacy remains to be demonstrated, and this will be the next challenge in future studies.

Materials and Methods
Patients
A total of 47 HCC patients who were eligible for surgical tumor resection were enrolled in the study between June 2015 and November 2020. Paired fresh liver tumor and TFL tissues, cut out at a minimal distance of $\geq$1 cm from the tumor, were used for isolating TILs and intrahepatic lymphocytes. In addition, peripheral blood was collected on the day of resection. None of the patients received systemic anti-cancer therapy or immunosuppressive treatment at least 3 months before surgery. The clinical characteristics of the patients are summarized in Table 1. The study was approved by the local ethics committee, and all specimens were obtained after written informed consent.

Cell Preparation
Single cell suspensions from peripheral blood, tumors, and TFLs were obtained as described previously.[44] Fresh tissue was cut into small pieces and digested in Hanks' balanced salt solution with Ca^{2+} and Mg^{2+} (Sigma-Aldrich, Zwijndrecht, the Netherlands) with 0.125 mg/mL of collagenase IV (Sigma-Aldrich, St Louis, MO) and 0.2 mg/mL of DNase I (Roche, Basel, Switzerland) for 30 minutes at 37°C with magnetic bead stirring. Cell suspensions were filtered through 100 μm cell strainers (BD Biosciences, Belgium), and mononuclear cells were obtained by Ficoll density gradient centrifugation. CD45$^+$ DAPI$^-$ leukocytes were quantified by using a MACSQuant flow cytometer (Miltenyi Biotech, Gladbach, Germany) after being stained with a mixture of DAPI, CD3, and CD45 antibodies.

Polyclonal T-Cell Stimulation
TILs of HCC patients were suspended in RPMI medium supplemented with 10% normal human serum, 2 mmol/L L-glutamine, 50 mmol/L Hepes buffer, 1% penicillin-streptomycin, 5 mmol/L sodium pyruvate, and 1% minimum essential medium nonessential amino acids. Five $\times$ 10^4 CD45$^+$ TILs were seeded in each well of a 96-well

Figure 8. CD155 is present on tumor-infiltrating APCs and overexpressed on HCC tumor cells. (*A*) Percentages of B cells, cDC, and monocytes within CD45$^+$ cells from tumor, TFL, and blood. *Dots* represent individual patients, and *bars* show mean ± SEM. (*B*) Representative histograms of CD155 expression on tumor-infiltrating B cells, cDC, and monocytes. (*C*) Percentages of CD155$^+$ cells within APC subsets and MFI of CD155 on APCs in tumor, TFL, and blood. (*D*) Representative images of immunohistochemistry staining show CD155 expression in HCC tumor and paired TFL tissue. The immunostaining score for patient 1 was 3D in tumor and 1D in TFL. Tonsil served as both positive and negative control tissue. Scale bars are presented in each image. (*E*) The immunostaining score of CD155 in individual patients is presented (n = 97). Significance was assessed by Wilcoxon matched-pairs signed-rank test. Data are presented as mean ± SEM. *$P < .05$.
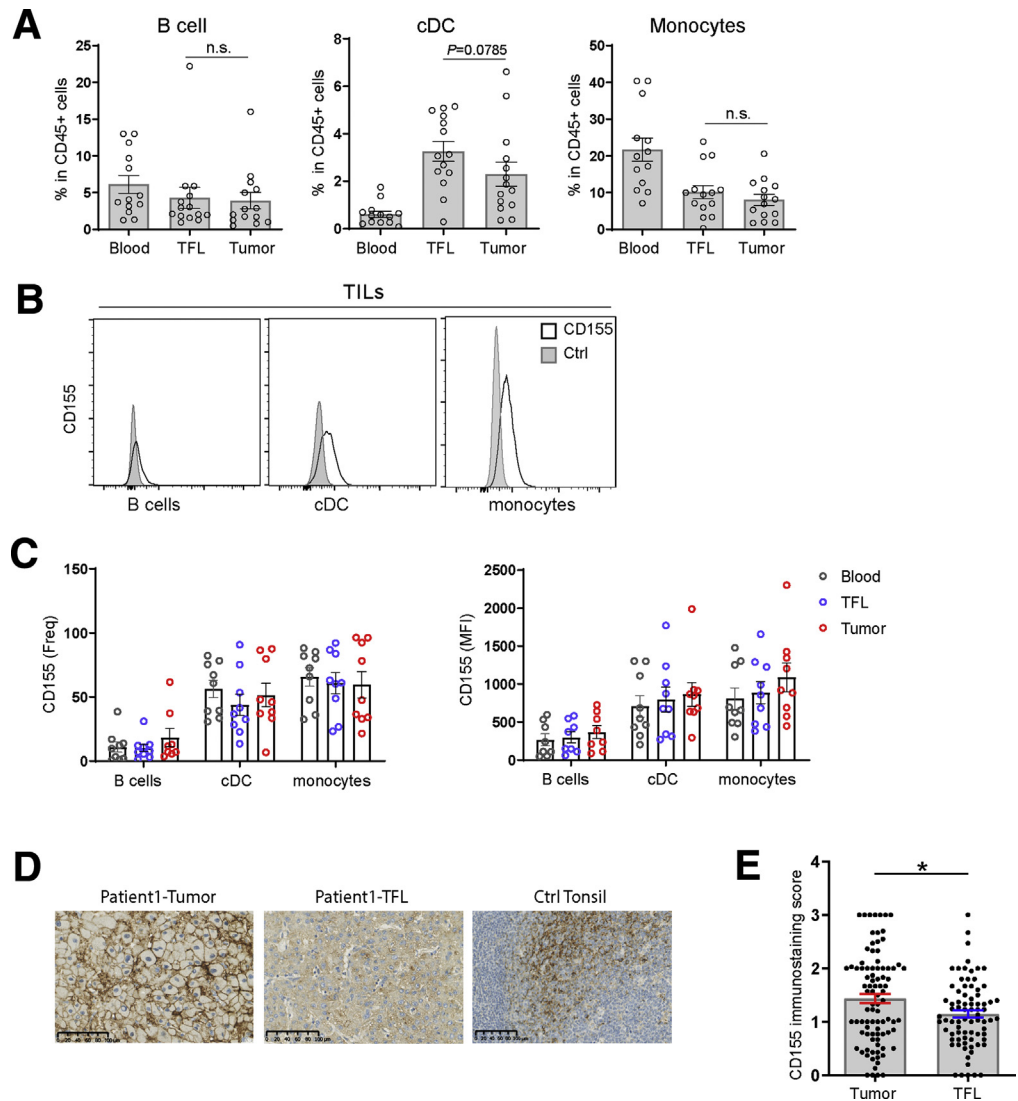
round-bottom culture plate and stimulated with a suboptimal amount of CD3/CD28 beads (beads to TILs ratio ranging from 1:10 to 1:800). Blocking mouse anti-human TIGIT antibody (clone MBSA43; eBioscience, San Diego, CA) was chosen on the basis of the referred article[45] and used at 10 and 20 μg/mL. Blocking human anti-human PD1 antibody (nivolumab; Bristol-Myers Squibb, New York, NY; provided by the Erasmus MC hospital pharmacy) was used at 10 μg/mL, which was based on the referred article.[46] Blocking anti-CD226 antibody clone DX11 (BD Biosciences) was used at 20 μg/mL according to previous studies.[19,47,48] Isotype control antibodies mIgG1 (clone MOPC-21; BioLegend, San Diego, CA) and hIgG4 (clone QA16A15; BioLegend) were added at 20 μg/mL and 10 μg/mL, respectively. T-cell proliferation was determined after 4 days of culture based on Ki67-expression in CD3$^+$ CD8$^+$ T cells on a FACSCanto II flow cytometer and analyzed by using FlowJo software version 10 (Tree Star Software, Ashland, OR). Dead cells

were excluded by Aqua live/dead fixable dye (Thermo Fisher Scientific, Waltham, MA) according to manufacturer's instructions. To measure intracellular IFN-γ produced by CD8$^+$ TILs, TILs were restimulated with anti-CD3/CD28 beads on day 3 after polyclonal stimulation, and Golgistop (containing monensin) was added (1:1500 dilution; BD Biosciences). After additional 24 hours of incubation, TILs were harvested and subjected to intracellular cytokine staining.

Antigen-Specific Stimulation

To test the effects of dual TIGIT/PD1 blockade on tumor-specific T-cell immunity, we used an antigen-specific assay as described in our previous HCC research.[11,49] Briefly, autologous B-cell blasts served as APCs and were electroporated with mRNA encoding GPC3 or MAGEC2, two tumor antigens that are frequently expressed in HCC tumors.[36] Importantly, the sequences encoding the tumor antigens in

the mRNAs are directly followed by a sequence encoding the transmembrane and luminal regions for DC-Lamp, which is a targeting signal for the endolysosomal compartment resulting in peptide loading in MHC class II as well as in MHC class I and thereby presentation to CD4$^+$ and CD8$^+$ T cells. TILs were stained with CFSE and co-cultured with
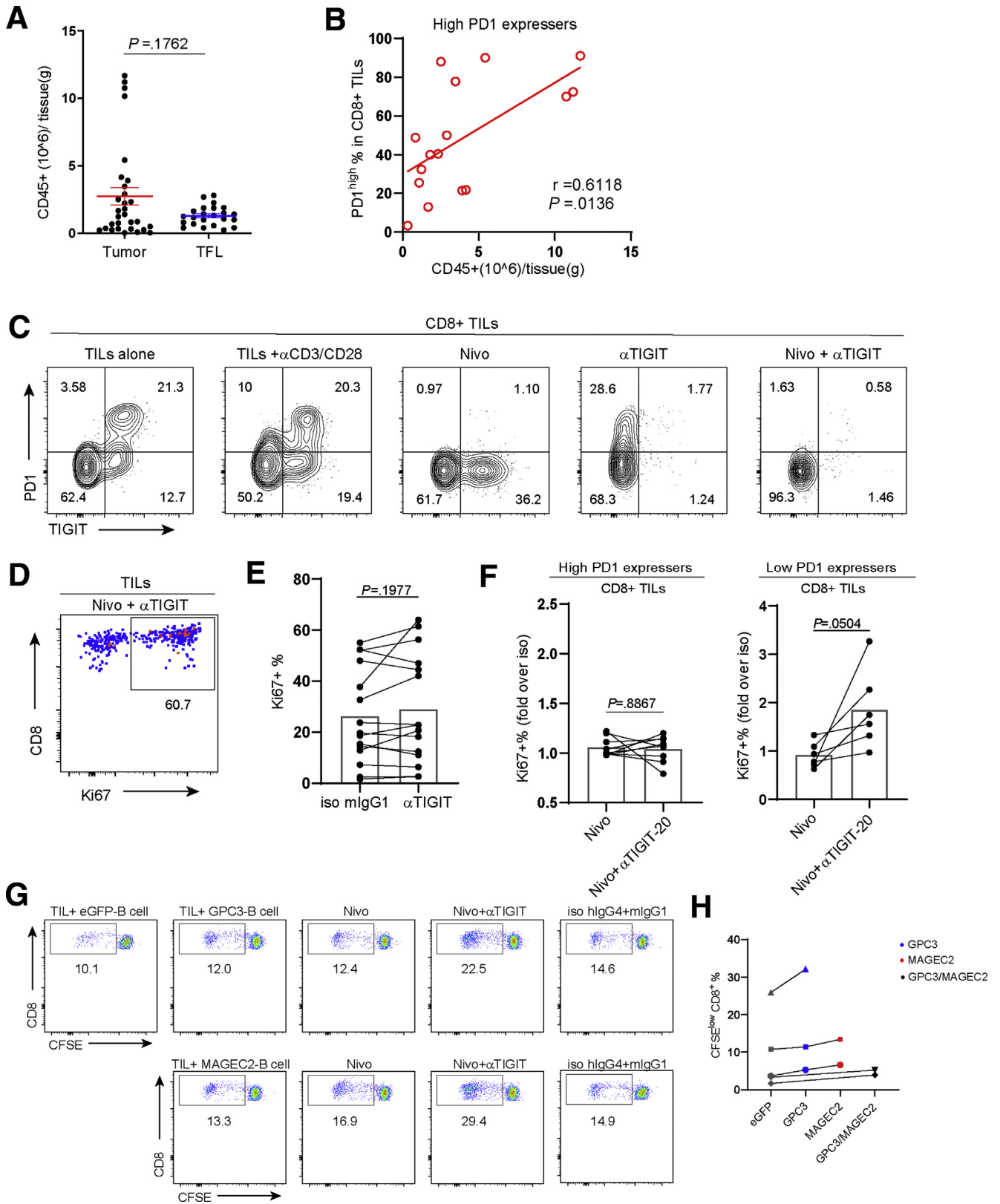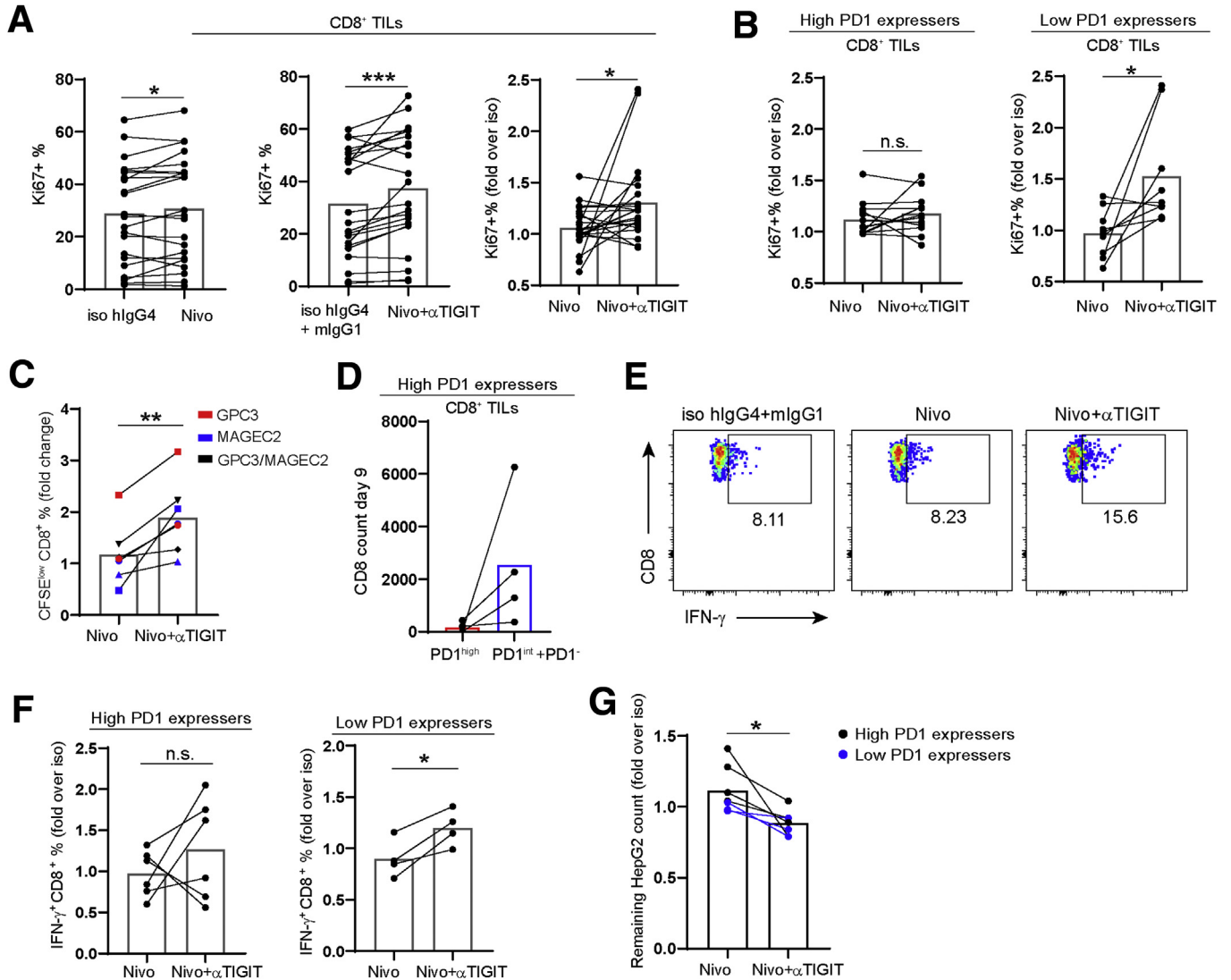
Figure 10. Combined TIGIT and PD1 blockade further enhances ex vivo functionality of CD8$^+$ TILs. (*A*) Effects of nivolumab (Nivo) single blockade and combined blockade with mouse anti-human TIGIT monoclonal antibody on CD8$^+$ TIL proliferation from individual patients on anti-CD3/CD28 beads stimulation (n = 22). (*B*) Effects of nivolumab blockade alone or combined with TIGIT blockade on CD8$^+$ TIL proliferation in high or low PD1 expressers. Data were normalized to each corresponding isotype. (*C*) Proliferation (CFSE-low) of CD8$^+$ TILs of individual patients (2 high PD1 expressers and 3 low PD1 expressers) in response to GPC3 and/or MAGEC2 in presence or absence of blocking antibodies. *Shapes* indicate different patients. Data were normalized to isotype and shown as fold change. (*D*) Total cell count of sorted PD1^{high} and PD1^{int} plus PD1$^-$ CD8$^+$ TILs on day 9 with CD3/CD28 beads stimulation. *Bars* represent mean. (*E*) Flow cytometry plots of IFN-γ in CD8$^+$ TILs after restimulated with anti-CD3/CD28 beads in polyclonal stimulation. (*F*) Production of IFN-γ by CD8$^+$ TILs in high or low PD1 expressers after restimulated with anti-CD3/CD28 beads in polyclonal stimulation. (*G*) Percent of remaining HepG2 was calculated by HepG2 count in each condition divided by HepG2 count in TIL + HepG2 only, and then the killing ratio of Nivo or Nivo/anti-TIGIT was normalized to corresponding isotype (n = 7). *P < .05, **P < .01, ***P < .001.

Figure 9. (*See previous page*). **Single TIGIT blockade did not significantly increase CD8$^+$ TIL proliferation.** (*A*) The number of CD45$^+$ cells isolated per gram of tissue from tumor and TFL. *Dots* show individual patients. (*B*) Correlation of PD1^{high} CD8$^+$ T-cell frequency and CD45$^+$ cells per gram of tissue. (*C*) Flow cytometry plots show blockade of TIGIT and PD1 by anti-TIGIT and anti-PD1 antibodies after 4 days in culture. (*D*) Flow cytometry plots show the proliferating (Ki67 positive) CD8$^+$ TILs after 4 days of stimulation by CD3/CD28 beads. (*E*) Effects of mouse anti-human TIGIT monoclonal antibody (10 μg/mL) on CD8$^+$ TIL proliferation from individual patients on anti-CD3/CD28 beads stimulation. (*F*) Effects of nivolumab (Nivo) blockade and combined blockade with mouse anti-human TIGIT monoclonal antibody on proliferation of CD8$^+$ TILs from individual patients on anti-CD3/CD28 beads stimulation. Percentages of Ki67 were normalized to cultures to which the corresponding isotype control antibodies had been added. (*G*) Flow cytometry plots of CD8$^+$ TIL proliferation in response to MAGEC2, GPC3, or eGFP mRNA-transfected autologous B-cell blasts in presence or absence of blocking antibodies. (*H*) Proliferation (CFSE-low) of CD8$^+$ TILs of individual patients in response to eGFP, GPC3, or/and MAGEC2.
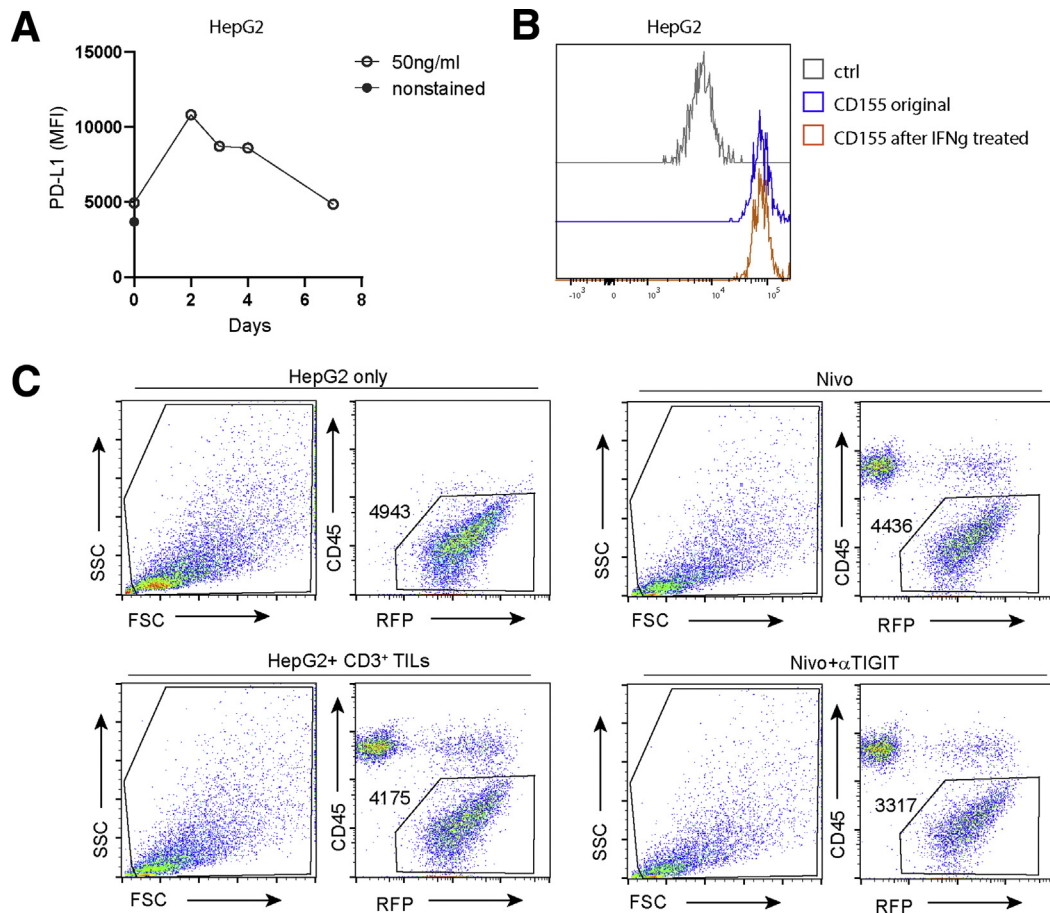
Figure 11. Expression of PD-L1 and CD155 on HepG2 and gating strategy for ex vivo cytotoxicity assay. (*A*) PD-L1 expression on HepG2 is shown over time after IFN-γ treatment. (*B*) Expression of CD155 on HepG2 without or with IFN-γ treatment is shown. (*C*) Flow cytometry plots of gating on HepG2 cells in ex vivo cytotoxicity assay. Number means HepG2 (CD45⁻RFP⁺) absolute count.

GPC3 mRNA- and/or MAGEC2 mRNA-, or eGFP (irrelevant control antigen) mRNA-transfected autologous B-cell blasts with a TIL:B cell ratio of 1:1, and proliferation of CD8$^+$ T cells was measured using flow cytometry on day 6.

Ex vivo Cytotoxicity Assay

HepG2 HCC cells expressing RFP-H2B on lentiviral transfection were used as target cells. RFP-H2B transduced cells give fluorescence in the Percp channel, thus enabling better differentiation between CD45$^+$ leukocytes and HepG2 cells. CD3$^+$ TILs isolated using CD3 microbeads (Miltenyi Biotec) were used as effector cells. HepG2 cells were pretreated with IFN-γ for 48 hours to induce PD-L1 expression. CD3$^+$ TILs were preactivated for 3 days with anti-CD3/CD28 beads and then co-cultured with IFN-γ-treated HepG2 cells in a ratio of 10:1 in absence or presence of nivolumab or nivolumab plus anti-TIGIT antibody, or corresponding isotype control antibodies (mentioned above). After 96 hours of co-culture, the remaining HepG2 cells were quantified using a MACSQuant flow cytometer.

PMA/Ionomycin Restimulation Assay

TILs were stimulated with PMA and ionomycin to assess effector cytokine production. Golgistop (containing monensin) was added (1:1500 dilution; BD Biosciences). After exposure to PMA and ionomycin for 5 hours, intracellular IFN-γ and TNF-α were measured by flow cytometry.

Flow Cytometry Analysis

Peripheral blood mononuclear cells and mononuclear cells isolated from TFL or tumor were analyzed for expression of surface and intracellular markers using the following anti-human antibodies: anti-TIGIT, anti-CD226, anti-PD1, anti-CD155, anti-perforin, anti-granzyme B, anti-CD8, anti-CD4, anti-CD56, anti-CD45, anti-TIM3, anti-LAG3, anti-TOX, anti-Ki67, and anti-TCF1 (Table 2). Viability of cells was assessed using Aqua LIVE/DEAD dye (Thermo Fisher Scientific). Fixation and permeabilization were performed using the Fixation/Permeabilization kit (eBioscience). For intracellular cytokine staining, cells were treated with 40 ng/mL PMA (Sigma, Zwijndrecht, the Netherlands) and 1 μg/mL ionomycin (Sigma) at 37°C

Figure 12. Combined TIGIT and PD1 blockade enhances ex vivo functionality of CD8$^+$ TILs in nivolumab (Nivo) non-responders. (*A*) Stratification of nivolumab responders and non-responders on the basis of CD8$^+$ TIL proliferation. (*B*) Effects of nivolumab blockade alone or combined with TIGIT blockade on CD8$^+$ TIL proliferation in nivolumab responders or non-responders. (*C*) Production of IFN-γ by CD8$^+$ TILs in nivolumab responders or non-responders after restimulated with CD3/CD28 beads in polyclonal stimulation. (*D*) Percent of remaining HepG2 depicted as ratio of absolute HepG2 count in presence of TIL+ Nivo or Nivo/anti-TIGIT versus corresponding isotypes (n = 6). (*E*) Distribution of high and low PD1 expressers in nivolumab responders and non-responders. *Bars* represent mean. *$P < .05$, **$P < .01$, ***$P < .001$.
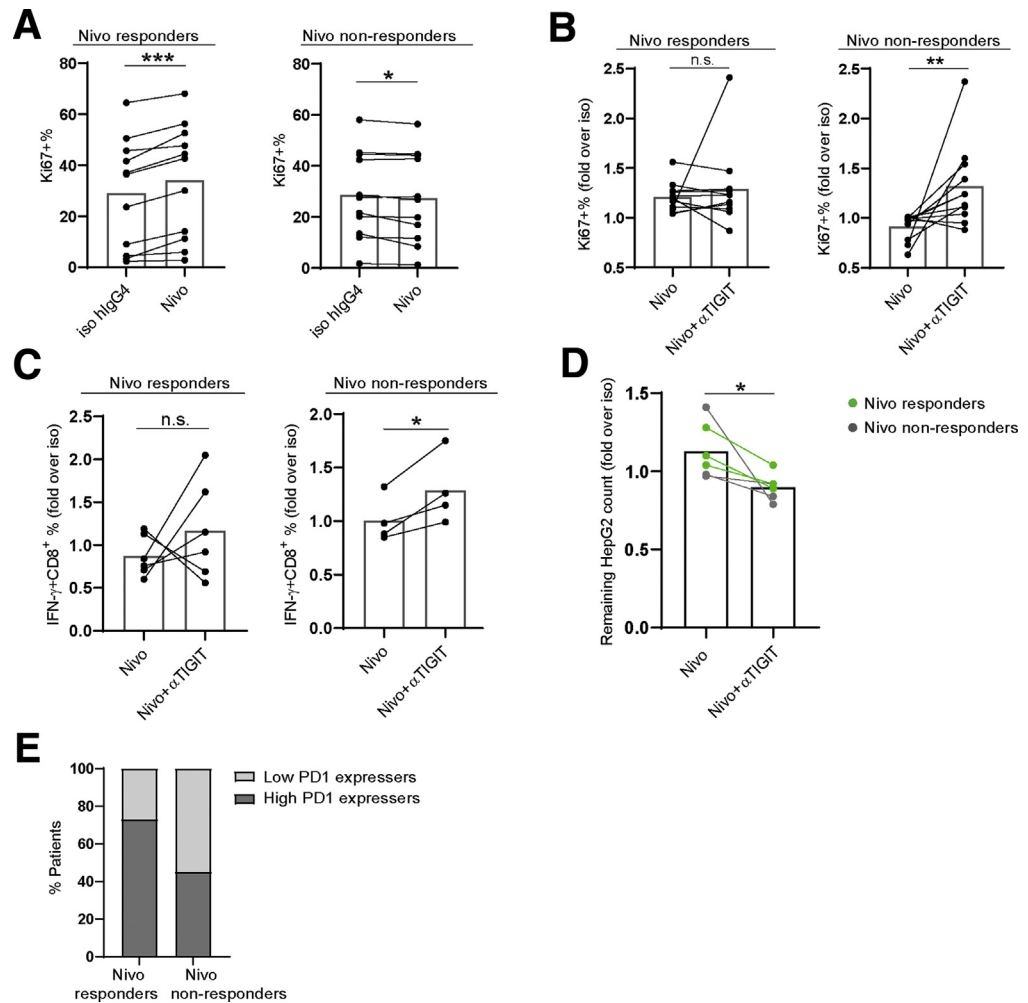
for 5 hours in the presence of GolgiStop at 1:1500 dilution (BD Biosciences), followed by staining of IFN-γ and TNF-α on fixed cells. Cells were analyzed using FACS-Canto II and Fortessa flow cytometers (BD Biosciences, San Diego, CA).

Flow Sorting

Frozen TILs were thawed and stained with anti-CD45-APC (clone HI30), anti-CD8-FITC (clone RPA-T8), and anti-PD1-PE (clone MIH4) antibodies. Dead cells were excluded by 7-AAD staining. PD1^{high} CD8$^+$ and PD1^{int} plus PD1$^-$ CD8$^+$ TILs were sorted separately into 2 fluorescence-activated cell sorter tubes. In addition, CD45$^+$ CD8$^-$ leukocytes from TILs were sorted. Cells were sorted using Aria II sorter (BD Biosciences).

Immunohistochemistry

The construction of TMAs of tumor and TFL tissues has been described previously.[35,36] The TMAs were then immunohistochemically stained by the Department of Pathology of Erasmus MC using rabbit anti-human monoclonal antibody CD155 (clone D3G7H, rabbit IgG, 1:400;

Cell Signaling Technology, Danvers, MA), which is the clone recommended by Chandramohan et al.[50] Immunohistochemistry was performed with an automated, validated, and accredited staining system (Ventana Benchmark ULTRA; Ventana Medical Systems, Tucson, AZ) using Optiview universal DAB detection Kit (#760-700). In brief, after deparaffinization and heat-induced antigen retrieval, the tissue samples were incubated according to their optimized time with CD155. Incubation was followed by hematoxylin II counter stain for 12 minutes and then a blue coloring reagent for 8 minutes according to the manufacturer's instructions (Ventana). The immunohistochemically stained TMAs were then scanned using NanoZoomer 2.0HT (Hamamatsu, Hamamatsu, Japan) and scored blindly by 2 researchers on the basis of the intensity of staining (0 [none], 1 [low], 2 [intermediate], 3 [strong]) and the frequency of positive tumor cells or hepatocytes (A [<10%], B [10%–50%], C [50%–90%], D [>90%]). The score per core was calculated by multiplying the intensity by the frequency of positive cells (A = 0.1, B = 0.3, C = 0.7, and D = 1), and then the average score per tissue was calculated by taking the average of the 3 scores.
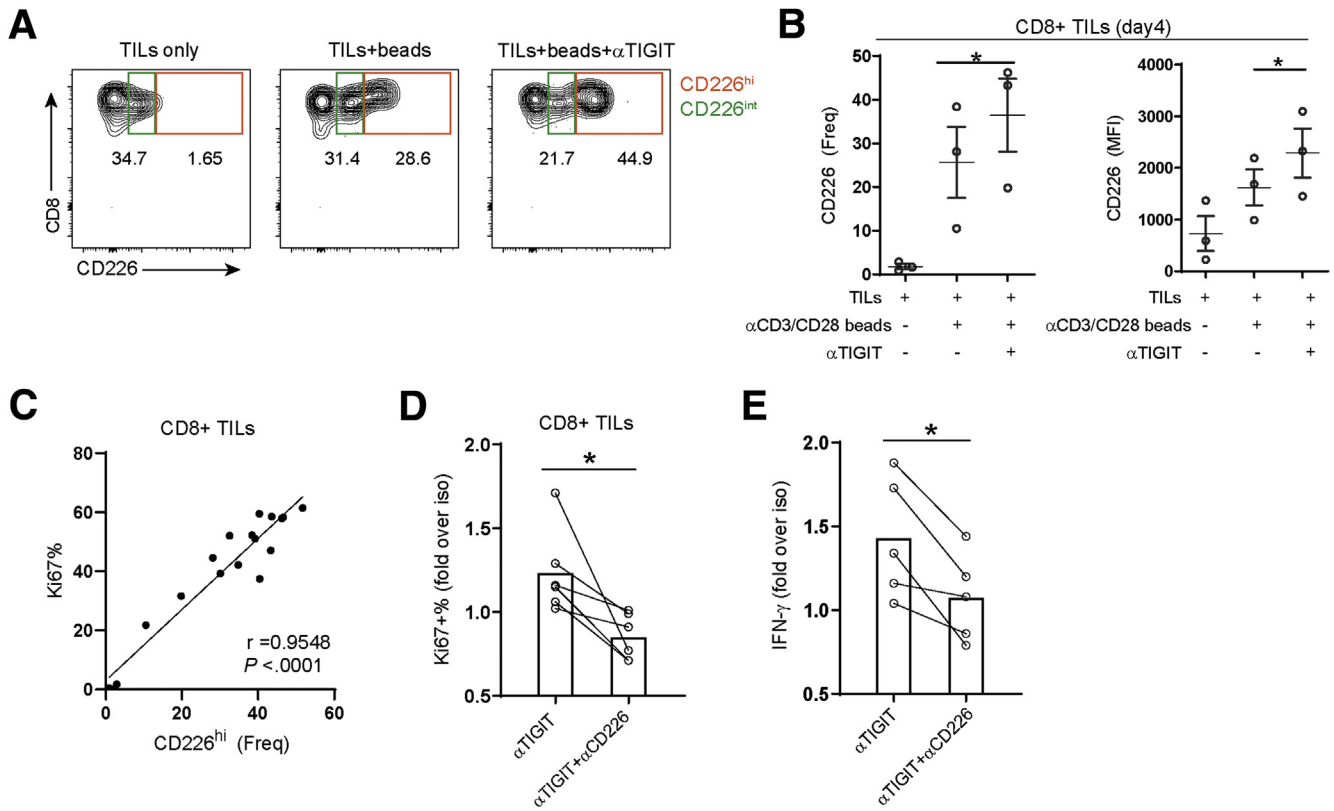
Figure 13. CD226 is required for the effect of TIGIT blockade. (*A*) Flow cytometry plots of CD226 expression on CD8$^+$ TILs after 4 days of cultures with/without CD3/CD28 beads stimulation or anti-TIGIT antibody. (*B*) Expression of CD226 on CD8$^+$ TILs after cultures with/without anti-CD3/CD28 beads stimulation or anti-TIGIT antibodies on day 4 (patients n = 3). Data are presented as mean ± SEM. (*C*) Correlation of Ki67% and CD226^{hi} frequencies in CD8$^+$ TILs after in vitro stimulation with CD3/CD28 beads. *Dots* show data from TILs that were involved in ex vivo polyclonal assays, including data from TIL only, TIL + beads, TIL + anti-TIGIT (10 and 20 μg/mL), or TIL + anti-PD1 + anti-TIGIT (10 and 20 μg/mL) (6 different conditions with n = 3 samples each, total 18). Significance was assessed by Pearson's correlation. (*D*) Proliferation of CD8$^+$ TILs stimulated with anti-CD3/CD28 beads in presence of anti-TIGIT or anti-TIGIT plus anti-CD226 antibodies (n = 6). (*E*) Production of IFN-γ by TILs stimulated with anti-CD3/CD28 beads in presence of anti-TIGIT or anti-TIGIT plus anti-CD226 antibodies (n = 5). Data normalized to each isotype. *P < .05. *Bars* represent mean.

Statistical Analysis

The distribution of all data sets was analyzed for normality using the Shapiro-Wilk test. The differences between paired groups of data were analyzed according to their distribution via paired *t* test or Wilcoxon matched-pairs test. Differences between different groups of patients were analyzed via *t* test or Mann-Whitney test. Spearman's rank correlation test for nonparametric data and Pearson's correlation test for parametric data were used to analyze the correlation between 2 factors. Statistical analysis was

Table 1. Patient Characteristics

	HCC patients[a] (n = 47)
Sex (male/female)	35/12
Age at surgery (y)[b]	67 ± 10
Race (white/Asian/black)	39/4/4
Cirrhosis (yes/no)	17/30
Tumor size (cm)[b]	8.7 ± 5.5
Tumor number (1/2)	43/4
AFP level before resection (μg/L)<20/20–400/>400/unknown	26/8/12/1

[a]Etiology of liver disease: no known liver disease (n = 19), hepatitis B/C (n = 7/5), alcohol-related liver disease (n = 1), nonalcoholic steatohepatitis/nonalcoholic fatty liver disease (n = 15).
[b]Median ± standard deviation.

Table 2. Anti-Human Antibodies Used in Flow Cytometry (Fluorescence-Activated Cell Sorter)

Antibody	Clone	Supplier	Antibody	Clone	Supplier
TIGIT-PE	MBSA43	eBioscience	FOXP3-eFluor450	236A/E7	eBioscience
TIGIT-efluor450	MBSA43	eBioscience	Perforin-FITC	delta G9	eBioscience
CD226-APC	11A8	BioLegend	GranzymeB-V450	GB11	BD Biosciences
CD155-PE	2H7CD155	eBioscience	CD14-PerCPCy5.5	61D3	eBioscience
PD1-PECy7	J105	eBioscience	BDCA1-APC	AD5-8E7	Miltenyi
PD1-PE	MIH4	eBioscience	CD19-APCH7	SJ25C1	BD Biosciences
CD3-PE	UCHT1	eBioscience	CD45-APC	HI30	BioLegend
CD3-PECy7	UCHT1	eBioscience	CD45-eFluor450	HI30	eBioscience
CD3-PerCPCy5.5	SK7	BD Biosciences	LAG3-PerCPeF710	3D923H	eBioscience
CD3-APCeFluor780	SK7	eBioscience	TIM3-PECF594	7D3	BD Biosciences
CD3-APCR700	UCHT1	BD Biosciences	IFNg-FITC	25723.11	BD Biosciences
CD3-Pacific blue	UCHT1	BD Pharmingen	TNFa-PerCPCy5.5	Mab11	BioLegend
CD4-PE	13B8.2	Beckman	Ki67-FITC	20Raj1	eBioscience
CD4-APC	OKT4	BioLegend	Ki67-PECy7	20Raj1	eBioscience
CD4-APCeFluor780	OKT4	eBioscience	CD38-FITC	T16	Beckman
CD4-BV605	OKT4	BioLegend	HLA-DR-APC	LN3	eBioscience
CD4-eFluor450	OKT4	eBioscience	CD39-FITC	A1	BioLegend
CD8-PerCPCy5.5	RPA-T8	eBioscience	CD103-PECy7	Ber-ACT8	BioLegend
CD8-FITC	SK1	eBioscience	TOX-APC	REA473	Miltenyi
CD8-FITC	RPA-T8	eBioscience	TCF1-PE	7F11A10	BioLegend
CD8-APC	RPA-T8	BioLegend	hIgG1-APC	REA293	Miltenyi
CD8-eluor450	RPA-T8	eBioscience	mIgG1-PE	P3.6.2.8.1	eBioscience
CD56-FITC	TULY56	eBioscience	mIgG1-PECy7	MOPC-21	BioLegend
CD56-BV510	HCD56	BioLegend	mIgG2b-FITC	27-35	BD Pharmingen

performed by using GraphPad (San Diego, CA) Prism 8.0. *P* value less than .05 was considered statistically significant (*$P < .05$, **$P < .01$, ***$P < .001$, ****$P < .0001$).

References

1. Bray F, Ferlay J, Soerjomataram I, Siegel RL, Torre LA, Jemal A. Global cancer statistics 2018: GLOBOCAN estimates of incidence and mortality worldwide for 36 cancers in 185 countries. CA Cancer J Clin 2018; 68:394–424.

2. El-Serag HB, Marrero JA, Rudolph L, Reddy KR. Diagnosis and treatment of hepatocellular carcinoma. Gastroenterology 2008;134:1752–1763.

3. El-Khoueiry AB, Sangro B, Yau T, Crocenzi TS, Kudo M, Hsu C, Kim T-Y, Choo S-P, Trojan J, Welling TH, Meyer T, Kang Y-K, Yeo W, Chopra A, Anderson J, dela Cruz C, Lang L, Neely J, Tang H, Dastani HB, Melero I. Nivolumab in patients with advanced hepatocellular carcinoma (CheckMate 040): an open-label, non-comparative, phase 1/2 dose escalation and expansion trial. Lancet 2017;389:2492–2502.

4. Zhu AX, Finn RS, Edeline J, Cattan S, Ogasawara S, Palmer D, Verslype C, Zagonel V, Fartoux L, Vogel A, Sarker D, Verset G, Chan SL, Knox J, Daniele B, Webber AL, Ebbinghaus SW, Ma J, Siegel AB, Cheng AL, Kudo M, investigators K-. Pembrolizumab in patients with advanced hepatocellular carcinoma previously treated with sorafenib (KEYNOTE-224): a non-randomised, open-label phase 2 trial. Lancet Oncol 2018;19:940–952.

5. Finn RS, Ryoo BY, Merle P, Kudo M, Bouattour M, Lim HY, Breder V, Edeline J, Chao Y, Ogasawara S, Yau T, Garrido M, Chan SL, Knox J, Daniele B, Ebbinghaus SW, Chen E, Siegel AB, Zhu AX, Cheng AL, investigators K-. Pembrolizumab as second-line therapy in patients with advanced hepatocellular carcinoma in KEYNOTE-240: a randomized, double-blind, phase III trial. J Clin Oncol 2020;38:193–202.

6. Boutros C, Tarhini A, Routier E, Lambotte O, Ladurie FL, Carbonnel F, Izzeddine H, Marabelle A, Champiat S, Berdelou A. Safety profiles of anti-CTLA-4 and anti-PD-1 antibodies alone and in combination. Nature Reviews Clinical Oncology 2016;13:473.

7. Larkin J, Chiarion-Sileni V, Gonzalez R, Grob JJ, Cowey CL, Lao CD, Schadendorf D, Dummer R, Smylie M, Rutkowski P. Combined nivolumab and ipilimumab or monotherapy in untreated melanoma. N Engl J Med 2015;373:23–34.

8. Hellmann MD, Paz-Ares L, Bernabe Caro R, Zurawski B, Kim S-W, Carcereny Costa E, Park K, Alexandru A, Lupinacci L, de la Mora Jimenez E, Sakai H, Albert I, Vergnenegre A, Peters S, Syrigos K, Barlesi F, Reck M, Borghaei H, Brahmer JR, O'Byrne KJ, Geese WJ, Bhagavatheeswaran P, Rabindran SK, Kasinathan RS, Nathan FE, Ramalingam SS. Nivolumab plus ipilimumab

in advanced non-small-cell lung cancer. N Engl J Med 2019;381:2020–2031.

9. Kim JE, Patel MA, Mangraviti A, Kim ES, Theodros D, Velarde E, Liu A, Sankey EW, Tam A, Xu H, Mathios D, Jackson CM, Harris-Bookman S, Garzon-Muvdi T, Sheu M, Martin AM, Tyler BM, Tran PT, Ye X, Olivi A, Taube JM, Burger PC, Drake CG, Brem H, Pardoll DM, Lim M. Combination therapy with anti-PD-1, anti-TIM-3, and focal radiation results in regression of murine gliomas. Clin Cancer Res 2017;23:124.

10. Sakuishi K, Apetoh L, Sullivan JM, Blazar BR, Kuchroo VK, Anderson AC. Targeting Tim-3 and PD-1 pathways to reverse T cell exhaustion and restore anti-tumor immunity. J Exp Med 2010;207:2187–2194.

11. Zhou G, Sprengers D, Boor PPC, Doukas M, Schutz H, Mancham S, Pedroza-Gonzalez A, Polak WG, de Jonge J, Gaspersz M, Dong H, Thielemans K, Pan Q, JNM IJ, Bruno MJ, Kwekkeboom J. Antibodies against immune checkpoint molecules restore functions of tumor-infiltrating T cells in hepatocellular carcinomas. Gastroenterology 2017;153:1107–1119 e10.

12. Yu X, Harden K, Gonzalez LC, Francesco M, Chiang E, Irving B, Tom I, Ivelja S, Refino CJ, Clark H, Eaton D, Grogan JL. The surface protein TIGIT suppresses T cell activation by promoting the generation of mature immunoregulatory dendritic cells. Nat Immunol 2009; 10:48–57.

13. Stanietsky N, Simic H, Arapovic J, Toporik A, Levy O, Novik A, Levine Z, Beiman M, Dassa L, Achdout H, Stern-Ginossar N, Tsukerman P, Jonjic S, Mandelboim O. The interaction of TIGIT with PVR and PVRL2 inhibits human NK cell cytotoxicity. Proc Natl Acad Sci U S A 2009;106:17858–17863.

14. Levin SD, Taft DW, Brandt CS, Bucher C, Howard ED, Chadwick EM, Johnston J, Hammond A, Bontadelli K, Ardourel D, Hebb L, Wolf A, Bukowski TR, Rixon MW, Kuijper JL, Ostrander CD, West JW, Bilsborough J, Fox B, Gao Z, Xu W, Ramsdell F, Blazar BR, Lewis KE. Vstm3 is a member of the CD28 family and an important modulator of T-cell function. Eur J Immunol 2011; 41:902–915.

15. Boles KS, Vermi W, Facchetti F, Fuchs A, Wilson TJ, Diacovo TG, Cella M, Colonna M. A novel molecular interaction for the adhesion of follicular CD4 T cells to follicular DC. Eur J Immunol 2009;39:695–703.

16. Fuchs A, Cella M, Giurisato E, Shaw AS, Colonna M. Cutting edge: CD96 (tactile) promotes NK cell-target cell adhesion by interacting with the poliovirus receptor (CD155). J Immunol 2004;172:3994.

17. Sakisaka T, Takai Y. Biology and pathology of nectins and nectin-like molecules. Curr Opin Cell Biol 2004; 16:513–521.

18. Joller N, Hafler JP, Brynedal B, Kassam N, Spoerl S, Levin SD, Sharpe AH, Kuchroo VK. Cutting edge: TIGIT has T cell-intrinsic inhibitory functions. J Immunol 2011; 186:1338–1342.

19. Lozano E, Dominguez-Villar M, Kuchroo V, Hafler DA. The TIGIT/CD226 axis regulates human T cell function. J Immunol 2012;188:3869–3875.

20. Johnston RJ, Comps-Agrar L, Hackney J, Yu X, Huseni M, Yang Y, Park S, Javinal V, Chiu H, Irving B, Eaton DL, Grogan JL. The immunoreceptor TIGIT regulates antitumor and antiviral CD8(+) T cell effector function. Cancer Cell 2014;26:923–937.

21. Josefsson SE, Huse K, Kolstad A, Beiske K, Pende D, Steen CB, Inderberg EM, Lingjærde OC, Østenstad B, Smeland EB, Levy R, Irish JM, Myklebust JH. T cells expressing checkpoint receptor TIGIT are enriched in follicular lymphoma tumors and characterized by reversible suppression of T-cell receptor signaling. Clin Cancer Res 2018;24:870–881.

22. Josefsson SE, Beiske K, Blaker YN, Førsund MS, Holte H, Østenstad B, Kimby E, Köksal H, Wälchli S, Bai B, Smeland EB, Levy R, Kolstad A, Huse K, Myklebust JH. TIGIT and PD-1 mark intratumoral T cells with reduced effector function in B-cell non-Hodgkin lymphoma. Cancer Immunology Research 2019; 7:355–362.

23. Chauvin JM, Pagliano O, Fourcade J, Sun Z, Wang H, Sander C, Kirkwood JM, Chen TH, Maurer M, Korman AJ, Zarour HM. TIGIT and PD-1 impair tumor antigen-specific CD8(+) T cells in melanoma patients. J Clin Invest 2015;125:2046–2058.

24. Dixon KO, Schorer M, Nevin J, Etminan Y, Amoozgar Z, Kondo T, Kurtulus S, Kassam N, Sobel RA, Fukumura D, Jain RK, Anderson AC, Kuchroo VK, Joller N. Functional anti-TIGIT antibodies regulate development of autoimmunity and antitumor immunity. J Immunol 2018; 200:3000–3007.

25. Kurtulus S, Sakuishi K, Ngiow SF, Joller N, Tan DJ, Teng MW, Smyth MJ, Kuchroo VK, Anderson AC. TIGIT predominantly regulates the immune response via regulatory T cells. J Clin Invest 2015;125:4053–4062.

26. Kim HD, Song GW, Park S, Jung MK, Kim MH, Kang HJ, Yoo C, Yi K, Kim KH, Eo S, Moon DB, Hong SM, Ju YS, Shin EC, Hwang S, Park SH. Association between expression level of PD1 by tumor-infiltrating CD8(+) T cells and features of hepatocellular carcinoma. Gastroenterology 2018;155:1936–1950 e17.

27. Ma J, Zheng B, Goswami S, Meng L, Zhang D, Cao C, Li T, Zhu F, Ma L, Zhang Z, Zhang S, Duan M, Chen Q, Gao Q, Zhang X. PD1(Hi) CD8(+) T cells correlate with exhausted signature and poor clinical outcome in hepatocellular carcinoma. J Immunother Cancer 2019; 7:331.

28. Scott AC, Dundar F, Zumbo P, Chandran SS, Klebanoff CA, Shakiba M, Trivedi P, Menocal L, Appleby H, Camara S, Zamarin D, Walther T, Snyder A, Femia MR, Comen EA, Wen HY, Hellmann MD, Anandasabapathy N, Liu Y, Altorki NK, Lauer P, Levy O, Glickman MS, Kaye J, Betel D, Philip M, Schietinger A. TOX is a critical regulator of tumour-specific T cell differentiation. Nature 2019;571:270–274.

29. Alfei F, Kanev K, Hofmann M, Wu M, Ghoneim HE, Roelli P, Utzschneider DT, von Hoesslin M, Cullen JG, Fan Y, Eisenberg V, Wohlleber D, Steiger K, Merkler D, Delorenzi M, Knolle PA, Cohen CJ, Thimme R, Youngblood B, Zehn D. TOX reinforces the phenotype

and longevity of exhausted T cells in chronic viral infection. Nature 2019;571:265–269.

30. Khan O, Giles JR, McDonald S, Manne S, Ngiow SF, Patel KP, Werner MT, Huang AC, Alexander KA, Wu JE, Attanasio J, Yan P, George SM, Bengsch B, Staupe RP, Donahue G, Xu W, Amaravadi RK, Xu X, Karakousis GC, Mitchell TC, Schuchter LM, Kaye J, Berger SL, Wherry EJ. TOX transcriptionally and epigenetically programs CD8(+) T cell exhaustion. Nature 2019; 571:211–218.

31. Siddiqui I, Schaeuble K, Chennupati V, Fuertes Marraco SA, Calderon-Copete S, Pais Ferreira D, Carmona SJ, Scarpellino L, Gfeller D, Pradervand S, Luther SA, Speiser DE, Held W. Intratumoral Tcf1(+)PD-1(+)CD8(+) T cells with stem-like properties promote tumor control in response to vaccination and checkpoint blockade immunotherapy. Immunity 2019;50:195–211. e10.

32. Chen Z, Ji Z, Ngiow SF, Manne S, Cai Z, Huang AC, Johnson J, Staupe RP, Bengsch B, Xu C, Yu S, Kurachi M, Herati RS, Vella LA, Baxter AE, Wu JE, Khan O, Beltra J-C, Giles JR, Stelekati E, McLane LM, Lau CW, Yang X, Berger SL, Vahedi G, Ji H, Wherry EJ. TCF-1-centered transcriptional network drives an effector versus exhausted CD8 T cell-fate decision. Immunity 2019;51:840–855.e5.

33. Im SJ, Hashimoto M, Gerner MY, Lee J, Kissick HT, Burger MC, Shan Q, Hale JS, Lee J, Nasti TH, Sharpe AH, Freeman GJ, Germain RN, Nakaya HI, Xue HH, Ahmed R. Defining CD8+ T cells that provide the proliferative burst after PD-1 therapy. Nature 2016; 537:417–421.

34. Duhen T, Duhen R, Montler R, Moses J, Moudgil T, de Miranda NF, Goodall CP, Blair TC, Fox BA, McDermott JE, Chang S-C, Grunkemeier G, Leidner R, Bell RB, Weinberg AD. Co-expression of CD39 and CD103 identifies tumor-reactive CD8 T cells in human solid tumors. Nature Communications 2018;9:2724.

35. Sideras K, Biermann K, Verheij J, Takkenberg BR, Mancham S, Hansen BE, Schutz HM, de Man RA, Sprengers D, Buschow SI, Verseput MC, Boor PP, Pan Q, van Gulik TM, Terkivatan T, Ijzermans JN, Beuers UH, Sleijfer S, Bruno MJ, Kwekkeboom J. PD-L1, galectin-9 and CD8(+) tumor-infiltrating lymphocytes are associated with survival in hepatocellular carcinoma. Oncoimmunology 2017;6:e1273309.

36. Sideras K, Bots SJ, Biermann K, Sprengers D, Polak WG, JN IJ, de Man RA, Pan Q, Sleijfer S, Bruno MJ, Kwekkeboom J. Tumour antigen expression in hepatocellular carcinoma in a low-endemic western area. Br J Cancer 2015;112:1911–1920.

37. Joller N, Lozano E, Burkett PR, Patel B, Xiao S, Zhu C, Xia J, Tan TG, Sefik E, Yajnik V, Sharpe AH, Quintana FJ, Mathis D, Benoist C, Hafler DA, Kuchroo VK. Treg cells expressing the coinhibitory molecule TIGIT selectively inhibit proinflammatory Th1 and Th17 cell responses. Immunity 2014;40:569–581.

38. Wang X, He Q, Shen H, Xia A, Tian W, Yu W, Sun B. TOX promotes the exhaustion of antitumor CD8+ T cells by preventing PD1 degradation in hepatocellular carcinoma. J Hepatol 2019;71:731–741.

39. Liu X, Li M, Wang X, Dang Z, Jiang Y, Wang X, Kong Y, Yang Z. PD-1(+) TIGIT(+) CD8(+) T cells are associated with pathogenesis and progression of patients with hepatitis B virus-related hepatocellular carcinoma. Cancer Immunol Immunother 2019;68:2041–2054.

40. Kim CG, Jang M, Kim Y, Leem G, Kim KH, Lee H, Kim T-S, Choi SJ, Kim H-D, Han JW, Kwon M, Kim JH, Lee AJ, Nam SK, Bae S-J, Lee SB, Shin SJ, Park SH, Ahn JB, Jung I, Lee KY, Park S-H, Kim H, Min BS, Shin E-C. VEGF-A drives TOX-dependent T cell exhaustion in anti–PD-1–resistant microsatellite stable colorectal cancers. Science Immunology 2019;4:eaay0555.

41. Ramsbottom KM, Hawkins ED, Shimoni R, McGrath M, Chan CJ, Russell SM, Smyth MJ, Oliaro J. Cutting edge: DNAX accessory molecule 1-deficient CD8+ T cells display immunological synapse defects that impair antitumor immunity. J Immunol 2014;192:553–557.

42. Duan X, Liu J, Cui J, Ma B, Zhou Q, Yang X, Lu Z, Du Y, Su C. Expression of TIGIT/CD155 and correlations with clinical pathological features in human hepatocellular carcinoma. Molecular Medicine Reports 2019; 20:3773–3781.

43. Sun H, Huang Q, Huang M, Wen H, Lin R, Zheng M, Qu K, Li K, Wei H, Xiao W, Sun R, Tian Z, Sun C. Human CD96 correlates to natural killer cell exhaustion and predicts the prognosis of human hepatocellular carcinoma. Hepatology 2019;70:168–183.

44. Pedroza-Gonzalez A, Verhoef C, Ijzermans JN, Peppelenbosch MP, Kwekkeboom J, Verheij J, Janssen HL, Sprengers D. Activated tumor-infiltrating CD4+ regulatory T cells restrain antitumor immunity in patients with primary or metastatic liver cancer. Hepatology 2013;57:183–194.

45. Inozume T, Yaguchi T, Furuta J, Harada K, Kawakami Y, Shimada S. Melanoma cells control antimelanoma CTL responses via interaction between TIGIT and CD155 in the effector phase. J Invest Dermatol 2016;136:255–263.

46. Wang C, Thudium KB, Han M, Wang XT, Huang H, Feingersh D, Garcia C, Wu Y, Kuhne M, Srinivasan M, Singh S, Wong S, Garner N, Leblanc H, Bunch RT, Blanset D, Selby MJ, Korman AJ. In vitro characterization of the anti-PD-1 antibody nivolumab, BMS-936558, and in vivo toxicology in non-human primates. Cancer Immunol Res 2014;2:846–856.

47. Ayano M, Tsukamoto H, Kohno K, Ueda N, Tanaka A, Mitoma H, Akahoshi M, Arinobu Y, Niiro H, Horiuchi T, Akashi K. Increased CD226 expression on CD8+ T cells is associated with upregulated cytokine production and endothelial cell injury in patients with systemic sclerosis. J Immunol 2015;195:892.

48. Boerman GH, van Ostaijen-ten Dam MM, Kraal KC, Santos SJ, Ball LM, Lankester AC, Schilham MW, Egeler RM, van Tol MJ. Role of NKG2D, DNAM-1 and natural cytotoxicity receptors in cytotoxicity toward rhabdomyosarcoma cell lines mediated by resting and IL-15-activated human natural killer cells. Cancer Immunol Immunother 2015;64:573–583.

49. van Beek AA, Zhou G, Doukas M, Boor PPC, Noordam L, Mancham S, Campos Carrascosa L, van der Heide-Mulder M, Polak WG, Ijzermans JNM, Pan Q, Heirman C, Mahne A, Bucktrout SL, Bruno MJ, Sprengers D, Kwekkeboom J. GITR ligation enhances functionality of tumor-infiltrating T cells in hepatocellular carcinoma. Int J Cancer 2019;145:1111–1124.

50. Chandramohan V, Bryant JD, Piao H, Keir ST, Lipp ES, Lefaivre M, Perkinson K, Bigner DD, Gromeier M, McLendon RE. Validation of an immunohistochemistry assay for detection of CD155, the poliovirus receptor, in malignant gliomas. Arch Pathol Lab Med 2017; 141:1697–1704.

Correspondence
Address correspondence to: Dave Sprengers, MD, PhD, Department of Gastroenterology and Hepatology, Erasmus MC-University Medical Center Rotterdam, Wytemaweg 80, 3015 CN Rotterdam, the Netherlands. e-mail: d.sprengers@erasmusmc.nl; fax: +31 10 7030352.